**NATIONAL UNIVERSITY OF SCIENCE AND TECHNOLOGY POLITEHNICA OF BUCHAREST**
**DOCTORAL SCHOOL OF MATERIALS SCIENCE AND ENGINEERING**
DEPARTMENT OF METALLIC MATERIALS SCIENCE, PHYSICAL METALLURGY

# PhD THESIS SUMMARY

# Mg-Zn-Ag ALLOYS FOR ORTHOPAEDICS IMPLANTS

**PhD Student: Dragomir (Nicolescu) Georgiana-Lavinia, Eng.**

**PhD Coordinator: Prof. Antoniac Vasile-Iulian, Eng., PhD**

| | | |
|---|---|---|
| **President** | Prof. Ghica Valeriu, eng., PhD | National University of Science and Technology Politehnica of Bucharest |
| **PhD Coordinator** | Prof. Antoniac Vasile Iulian, eng., PhD | National University of Science and Technology Politehnica of Bucharest |
| **Referents** | Prof. Mohan Aurel, eng., PhD | University of Oradea |
| | Prof. Popescu Violeta, eng., PhD | Technical University of Cluj-Napoca |
| | Conf. Cotruț Cosmin-Mihai, eng., PhD | National University of Science and Technology Politehnica of Bucharest |

**BUCHAREST**

**2023**

# SUMMARY

# ACKNOWLEDGEMENT

At the end of this important stage in my life, I would like to thank to those who guided me or have been with me throughout this period.

Cordial thanks to the PhD coordinator, Prof. habil. Vasile-Iulian Antoniac, eng., PhD, from National University of Science and Technology Politehnica of Bucharest, Faculty of Materials Science and Engineering, for the contribution made in my evolution as a teacher, coordinator, scientific researcher, mentor, for the permanent support, involvement and dedication for the valuable scientific advice granted during the entire period of research and development of the doctoral thesis, but also in personal development.

All my respect and gratitude to the professors from the Department of Metallic Materials Science, Physical Metallurgy, Faculty of Materials Science and Engineering, National University of Science and Technology Politehnica of Bucharest, who shared their knowledge that led me towards scientific research and ensured my access to the necessary equipment for conducting experimental research.

Also, I would like to express my special thanks to the scientific researcher Dr. Eng. Alina Vlădescu (Dragomir) from the National Research and Development Institute for Optoelectronics, the scientific researcher Irina Titorencu from the "Nicolae Simionescu" Institute of Cellular Biology and Pathology and Prof. Habil. Florin Miculescu, eng., PhD, for involvement, invaluable help and support from technical-scientific point of view, and access to the experimental facilities in the laboratories they coordinate.

I thank and appreciate the continuous support of the steering committee members during the doctoral stage, namely Prof. Brandușa Ghiban, eng., PhD, associate professor Cosmin-Mihai Cotruț, eng., PhD, assistant prof. Diana Vrânceanu, eng., PhD, for their help and valuable scientific advice.

I have a special gratitude for the scientific researcher Dr. Eng. Aurora Antoniac, whom I thank for her trust and support, and for the valuable advice given constantly throughout the period of my doctoral studies.

I thank my parents, especially my mother, for her attention, guidance and unconditional love. From her I learned that simplicity and modesty will never fail, always emphasizing the importance of a good education.

I thank my husband, Cosmin Nicolescu, for the unconditional support, trust and encouragement offered throughout my doctoral studies.

With special gratitude and love, I dedicate this thesis to my parents, Ioana and Petruș Dragomir, and my husband, Cosmin Nicolescu, because they represent my moral support in life, they have been by my side and surrounded me with affection and patience.

# ABSTRACT

This doctoral thesis includes both a theoretical study and a series of experimental research carried out with the aim of characterization and testing of two experimental magnesium alloys from the system Mg–Zn–Ag as a possible solution to manufacturing the orthopedic implants.

Biodegradable magnesium-based alloys represent the new generation of biodegradable metallic biomaterials with good osseointegration property. Compared to other metallic biomaterials used for orthopedic implants, such as titanium and titanium alloys, stainless steels or cobalt-chromium alloys, magnesium alloys stand out for their low elasticity modulus, similar to human bone, which prevents stress shielding effect, as well as their biodegradability character. The main limitation of magnesium and its alloys is represented by rapid degradation, thus requiring a rigorous control of the corrosion rate that is consistent with the repair and regeneration of the affected bone tissue. The rapid corrosion process involves other consequences for the implant, such as the loss of mechanical properties, as well as for the biological environment, through toxic effects due to secondary reactions and the accumulation of corrosion sub products. Thus, there are major implications in the medical cost of the operation, but also in the health of the patients. Therefore, in such applications it is necessary to improve the corrosion resistance of Mg alloys.

Thus, the objectives of this thesis were to evaluate the potential of two experimental magnesium alloys from the system Mg–Zn–Ag as a possible solution to manufacturing the orthopedic implants, as well as the evaluation of the effect of hydroxyapatite coatings deposited by the radio-frequency magnetron sputtering method at 300°C, as a solution for controlling the degradation of the above-mentioned magnesium-based alloys and their biocompatibility. For this evaluation, the electrochemical and immersion tests were used to determine their corrosion resistance while being immersed in a simulated body fluid solution, and the biocompatibility testing. In conclusion, the experimental magnesium alloys from the system Mg–Zn–Ag coated with hydroxyapatite show a higher potential to be used to manufacturing the orthopedic implants.

**Keywords**: Mg-based alloys, hydroxyapatite, magnetron sputtering, biodegradation

# INTRODUCTION

The need to repair and regenerate bone tissues has inspired the research and the development of a large number of medical materials and devices for bone repair. Bone repair is a physiological process influenced by a variety of biomechanical, biochemical, cellular, hormonal, and pathological factors. A large number of bone repair materials have been increasingly used. The metal materials currently widely used in the execution of implants for osteosynthesis are stainless steels and titanium alloys, because they have adequate mechanical properties, acceptable corrosion resistance and are biocompatible. However, problems related to the release of metal ions, corrosion and wear, which trigger inflammatory tissue responses, have been reported. In addition, the elastic modulus of the bones is different and thus stress shielding occurs which leads to the loss of surrounding bone tissue. Perhaps the most important disadvantage of these implants is that they must be removed through secondary surgery once the bone fracture has completely healed. In order to minimize patient trauma and reduce medical costs, attempts have been made in recent years to develop new materials and biodegradable osteosynthesis implants to eliminate the need for secondary surgical interventions.

An important class of biodegradable metallic materials with great potential to be used in the execution of implants for osteosynthesis is represented by magnesium alloys, because they are biodegradable in the human body, do not show toxicity and have acceptable mechanical properties. Magnesium is an essential element in many metabolic processes and is mainly stored in bone tissue, stimulates the growth of bone cells and accelerates the healing of bone tissue. Mg alloys are degraded *in vivo* due to the presence of $Cl^-$ in the physiological environment, thus eliminating the need for secondary surgical interventions for implant removal. $Mg^{2+}$ ions, released as a result of the degradation of Mg alloy implants, do not cause complications because the excess is eliminated through urine.

Although numerous experimental researches and publications are reported on the potential use of several magnesium alloys as osteosynthesis implants, a translation to the actual execution of implants at an industrial level has not been achieved. This is because a number of problems still persist, such as the too rapid degradation of these materials inside the human body and the mismatch of the rate of implant degradation with the healing rate of the bone tissue, which generally consists of an early inflammatory stage lasting from 3 to 7 days, a reparative stage that leads to strong healing that lasts about 3-4 months, and then a remodelling phase that can last months to years. Other problems identified by many researchers relate to the fact that the rapid degradation of magnesium alloys results in the formation of hydrogen gas cavities, rapid loss of mechanical integrity of implants, and adverse reactions of the host tissue after surgery.

In this doctoral thesis, experimental studies and research were carried out regarding magnesium alloys potentially usable as biomaterials, in order to obtain orthopaedic implants for fracture fixation, two magnesium alloys from the Mg-Zn-Ag ternary system being selected. A complex microstructural characterization of two alloys from the Mg-Zn-Ag system, respectively Mg7Zn1Ag and Mg6Zn3Ag, was carried out, following the structural factors that influence the corrosion of magnesium alloys, respectively the microstructural uniformity, the grain size and the secondary phases present in the microstructure, but also the effect of Ag addition on these microstructural characteristics. The complex characterization was carried out using modern methods, namely scanning electron microscopy coupled with EDS spectrometry, X-ray diffraction and optical microscopy.

Due to the rapid biodegradation of these alloys in the human body and in simulated environments, hydroxyapatite coating of experimental magnesium alloys was used.

Hydroxyapatite coatings on Mg-Zn-Ag magnesium alloy were prepared by the magnetron sputtering method in radio frequency mode at a deposition temperature of 300°C. The deposition temperature of 300°C was sufficient to obtain a crystalline hydroxyapatite structure with a Ca/P ratio close to the stoichiometric one. The adhesion of the coatings was not influenced by the nature of the Mg–Zn–Ag alloys, so similar values were found for both coated alloys. The experimental results showed that the coating layer was homogeneously deposited on the Mg-Zn-Ag alloys.

In the last part of the paper, the functional testing of Mg-Zn-Ag magnesium alloys coated with hydroxyapatite is presented, respectively the evaluation of the in vitro biocompatibility properties through cytotoxicity tests, and the evaluation of the corrosion resistance of the alloys through electrochemical tests, immersion tests, and by determining the amount of hydrogen released.

The chapter structure of this doctoral thesis is as follows:

**THEORETICAL PART**

**Chapter 1** - "*The current state of research on the types of magnesium alloys potentially usable as biomaterials*" contains the latest information on the current state of magnesium alloys and their potential clinical applications. This chapter describes the most important magnesium alloys and the influence of alloying elements, specific aspects regarding the degradation of magnesium alloys, as well as the most important biomedical applications. A subchapter is dedicated to the influence of silver as an alloying element in magnesium alloys for orthopaedic implants with antibacterial properties, a novel element in the landscape of research on biodegradable magnesium alloys for orthopaedic implants.

**Chapter 2** - "*Methods of modifying the surface of biodegradable magnesium alloys*" presents general notions regarding the main methods of modifying the surface of magnesium alloys, classifications, but also information on the current state of hydroxyapatite coatings for biodegradable magnesium alloys.

**EXPERIMENTAL PART**

**Chapter 3** - "*Research methodology*" presents the purpose of the work, the experimental materials used in the research, the work plan, the analysis methods and the equipment used for characterization and testing.

**Chapter 4** - "*Structural characterization of some magnesium alloys from the Mg-Zn-Ag system usable in traumatology*" describes the microstructural characterization of the experimental samples from the experimental Mg-Zn-Ag alloys, with the help of scanning electron microscopy coupled with EDS spectrometry, diffraction of X-ray and optical microscopy.

**Chapter 5** - "*Modification of the surface of Mg-Zn-Ag magnesium alloys by the deposition of hydroxyapatite using the magnetron sputtering method and their characterization*" presents the experimental work method and the equipment used to modify the surface of the experimental Mg-Zn-Ag alloys by the deposition of hydroxyapatite by the magnetron sputtering method in radio frequency mode, but also the structural characterization of the deposited hydroxyapatite film and their surface properties.

**Chapter 6** - "*Functional testing of Mg-Zn-Ag magnesium alloys*" includes the evaluation of the *in vitro* biocompatibility properties of the alloys by cytotoxicity tests, but also the evaluation of the corrosion resistance of the alloys by immersion, electrochemical tests and by determining the amount of hydrogen released.

**Conclusions** include the presentation of general conclusions, but also original contributions and the dissemination of the results obtained. At the end, the bibliographic references, an index of figures and an index of tables are presented.

# CHAPTER 1. CURRENT STATE OF RESEARCH ON THE TYPES OF MAGNESIUM ALLOYS POTENTIALLY USABLE AS BIOMATERIALS

## 1.1.Magnesium alloys and the influence of alloying elements

Many people suffer bone fractures each year from accidents or disease. Most of these fractures are too complex to be solved by external medical treatment, which is why they must be fixed surgically with implants. Traditional methods of osteosynthesis or osteotomy are used to fix the bone, permanent metal implants such as screws and plates made of steel or titanium alloys, which are then excised. This is especially necessary in young, growing patients. Usually, permanent metal implants are removed one or two years after the first surgery.

Magnesium-based alloys (Mg) currently represent a new generation of biodegradable metallic materials with excellent osseointegration properties and could be used in the execution of orthopaedic implants, alongside the traditional metallic biomaterials represented by titanium and titanium alloys, stainless steels and cobalt-chromium alloys. Figure 1.1 shows the properties of magnesium alloys in relation to other biomaterials used. Compared to other metallic materials, magnesium alloys stand out for their low elasticity, like that of human bone, which prevents the negative effect in the bone structure known as the stress shielding effect.

Recent studies pay special attention to magnesium-based alloys for medical applications, because they are light materials (with densities close to those of cortical bone 1.75– 2.1 g/cm$^3$) [10,20,21], with mechanical properties similar to human bone and are biodegradable. The last aspect is extremely important for surgical applications. Although considerable international effort is being devoted to the research and development of Mg-based alloys, the corrosion rates are still difficult to control and relatively high.

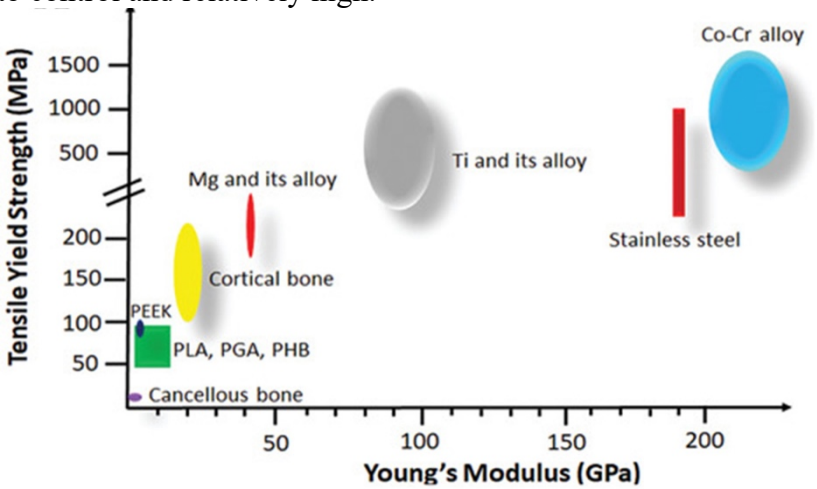


**Figure 1.1.** Mechanical properties of bone tissues and the main classes of biomaterials used for orthopaedic implants

To control the degradation rate of Mg-based implants, to maintain their mechanical strength during use and to reduce side effects, many Mg alloys have been designed for medical applications by adding different specific alloying elements [70 ]. Alloying elements have a direct impact on the corrosion resistance of Mg-based alloys [71]. The addition of suitable alloying elements can improve the mechanical properties of Mg and reduce the corrosion rate of Mg by changing the structure and phase distribution [72]. However, the long-term cytotoxicity and inflammatory consequences of these elements are also major concerns [73]. Therefore, alloying elements must be carefully selected to maintain the biocompatibility of the implants, as they also degrade in body fluids during the degradation process.

Figure 1.5 explains the evolution of improving the characteristics of magnesium alloys through the addition of alloying elements. If from a toxicological point of view, it is relatively

simple to select a series of potential alloying elements, from the point of view of the effects of the addition of different alloying elements and their proportion on the structural characteristics it is much more complicated. If in the case of binary magnesium alloys the results of various research groups signal progress in the field, ternary magnesium-based alloy systems or complex ones with several alloying elements are still being evaluated.

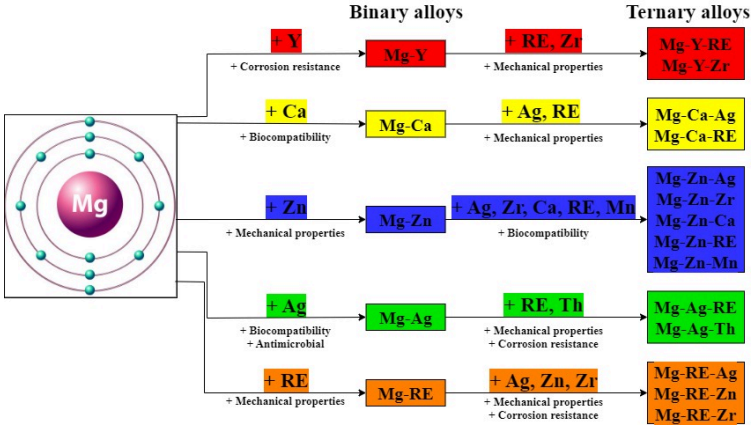


**Figure 1.5.** The progression of magnesium alloys with the addition of elements which lead to improved properties

## 1.2. Specific aspects regarding the biodegradation of magnesium alloys for biomedical applications

Despite remarkable progress in the development of Mg-based alloys, extensive clinical applications and commercialization of most Mg-based implants are still limited due to their uncontrollable degradation rate. The different types of corrosion generally observed for Mg implants in the body environment are illustrated schematically in Figure 1.6.

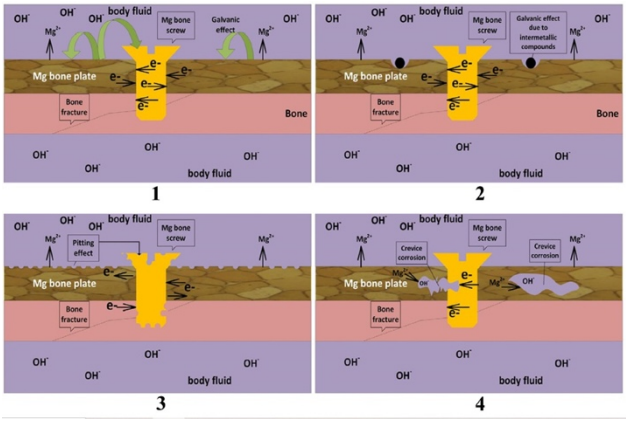


**Figure 1.6.** Schematic illustration of the major types of corrosion processes observed for magnesium implants in the body fluid environment
*1. galvanic effect on the implant, 2. galvanic corrosion due to intermetallic compounds, 3. "pitting" corrosion and 4. crevice corrosion* [10];

In orthopedic applications, implants are often required to provide resistance to certain mechanical stresses during the healing of damaged bone tissue. Although biodegradable implants are eventually allowed to degrade, they still need sufficient mechanical strength during use. An ideal situation is that the rate of degradation of the implant matches the rate of healing of the bone tissue. Nonuniform and local degradation behavior can also give rise to stress corrosion cracking, reduced mechanical strength, and unexpected breakage before the expected healing time, which negatively affects the durability of implants [78,134]. The

mechanical properties of the implants are insufficient before the host tissue is fully healed, ultimately leading to loss of mechanical integrity and failure of the implants.

## 1.3. Biomedical applications of magnesium alloys

Currently, applications of biomedical Mg alloys mainly include cardiovascular stents and bone implants [137,138].

Current clinical applications of magnesium-based orthopaedic implants remain relatively nascent and rare. Mg as an orthopaedic biomaterial has been reported to promote bone remodelling and healing [58]. Notable implants in recent years include MAGNEZIX® (Syntellix AG, Hannover, Germany) MgYREZr bioresorbable alloy compression screw and K-MET™ bioresorbable bone screw (U&i Corporation, Seoul, Korea), and both have demonstrated positive clinical results in many clinical applications.

Currently, there are limited applications for magnesium and its alloys in cardiovascular surgery. Magnesium and its alloys are being investigated for their ability to replace bio-inert metal implants in typical cardiovascular therapeutic applications. These include prosthetic implantation and stenting, such as artificial valves, stents, pacemaker casings, and stent grafts.

In 2016, DREAMS 2G (Magmaris) stent from Biotronik, a German company, obtained a CE certificate. Biotronik's Magmaris BRS is made of MgYREZR alloy and has been used in clinical applications. Haude et al. found that the second-generation absorbable drug-eluting Mg-alloy stent (DREAMS 2G) showed significant performance in blood vessels and was implanted in 123 patients with obstructive coronary artery disease. Only four (<4%) patients showed abnormalities. Angiography of the remaining patients identified vascular motion. In addition, optical coherence tomography did not detect any intraluminal mass or thrombosis.

Figure 1.10 provides examples of commercial resorbable metal implants made of Mg and its alloys.


**Figure 1.10**. Examples of commercial implants made of biodegradable magnesium alloys

## 1.4. Current status on the use of silver as an alloying element in magnesium alloys for orthopaedic implants with antibacterial properties

The use of silver as an alloying element in biodegradable magnesium alloys has relatively recently attracted the attention of researchers in the field. Not only is it a biocompatible element, but it has the ability to modify the microstructure and thereby improve the mechanical properties and degradation behaviour [143,144].

Alloying with antimicrobial elements such as Ag, Ga and Cu has been reported as a suitable approach to develop biodegradable Mg implants with suitable antibacterial properties. The addition of Ag has been reported to cause a remarkable decrease in the grain size of pure Mg, resulting in improved mechanical properties.

The corrosion behaviour of Ag-incorporated Mg-based biodegradable alloys is mainly governed by the following three factors: (1) the volume fraction and distribution of Ag-containing secondary phases, where these phases can act as a cathode and accelerate the micro-galvanic corrosion, (2) the presence of Ag as a dissolved element in the Mg network, which can promote corrosion resistance by improving the standard electrode potential of the alloy, and (3) grain size.

Three main mechanisms have been proposed for the antibacterial activities of $Ag^+$ ions: (1) disruption of the bacterial membrane by $Ag^+$ ions, where they can be absorbed by the sulfur-containing cell membrane (which is negatively charged) by electrostatic attraction, leading to serious damage to the cell membrane. The negative charge of the cellular wall would be changed by the adsorption of Ag particles, leading to the polarization of the cellular wall. In this case, the blurred appearance of the bacterial cell wall indicates its degradation, as seen under a laser scanning confocal microscope.

Figure 1.11. presents a schematic illustration of the discussed antibacterial mechanisms of Ag-containing biodegradable implants, where $Ag^+$ ions will be released throughout the degradation period of the implant, causing the establishment of a microenvironment in the vicinity of the implantation site with a constant concentration of $Ag^+$ ions [144].

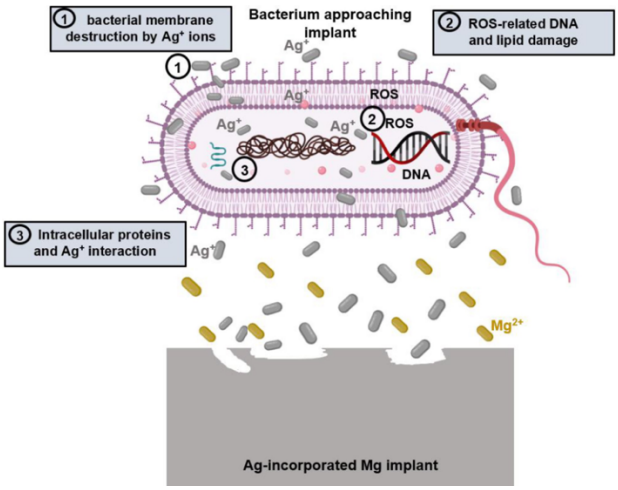


**Figure 1.11.** Schematic illustration of the antibacterial mechanisms of the biodegradable magnesium (Mg) alloy implant that also contains silver (Ag)

# CHAPTER 2. METHODS OF MODIFICATION OF THE SURFACE OF BIODEGRADABLE MAGNESIUM ALLOYS

## 2.1. Surface modification methods for biodegradable magnesium alloys

Surface modification is one of the most effective ways to control and reduce the degradation rate of Mg to improve the corrosion resistance of Mg surface. Surface modification of the Mg substrate can effectively isolate or reduce the contact area between the substrate and body fluid, which is useful for maintaining the mechanical integrity of the Mg implant before a bone lesion is completely healed. According to different modification methods, surface modification can be divided into four categories: chemical modification, physical modification, compound modification, and other surface treatments, as shown in Figure 2.1 [133].

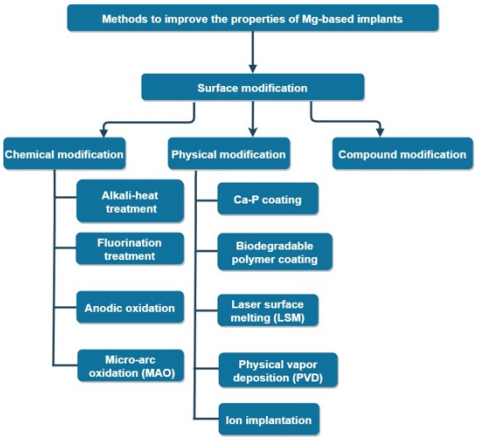


**Figure 2.1.** Classification of surface modification methods to improve the properties of magnesium alloy implants [133]

### 2.2. Current status of hydroxyapatite coatings for biodegradable magnesium alloys

Hydroxyapatite (HA) is a bioceramic material ($Ca_{10}(PO_4)_6(OH)_2$), which has a hexagonal crystal structure. The lattice parameters are: a = b = 0.943 nm, c = 0.688 nm, the angle between the a and b axes is 120°, and the unit cell contains 10 $Ca^{2+}$, 6 $PO_4^{3-}$ and 2 $OH^-$. The Ca/P atomic ratio is 1.67, and it is the main component of natural bones. It has excellent bioactivity and osteoconductivity, so it can quickly integrate with bones and promote new bone growth. Currently, it is considered an important material in the field of biomaterials and also has a huge development potential [159–161]. The most widely used application of HA is in the coating of metal implants.

Various coating techniques are available, including chemical [62], hydrothermal [162], electrochemical deposition [163], plasma jet deposition [164], ion implantation [165], sputtering [166], and sol-gel methods [ 167]. Because some of these methods operate at high temperatures, it is extremely difficult to deposit HA on magnesium-based materials.

## CHAPTER 3. RESEARCH METHODOLOGY

### 3.1. The purpose of the work, the experimental materials and the work plan

The main objectives of this doctoral thesis were to evaluate the potential of some innovative magnesium alloys, from the Mg-Zn-Ag alloy system, to be used in the execution of osteosynthesis implants, as well as to determine the effect induced by the coating of these alloys with hydroxyapatite, by the radiofrequency magnetron sputtering method at a deposition temperature of 300°C, on the biodegradation and biocompatibility of these alloys, in order to meet the functional requirements of biodegradation in a biological environment imposed by their use in the execution of temporary orthopaedic implants.

In order to achieve the main objective of this work, several stages were completed which can be found in the following figure:

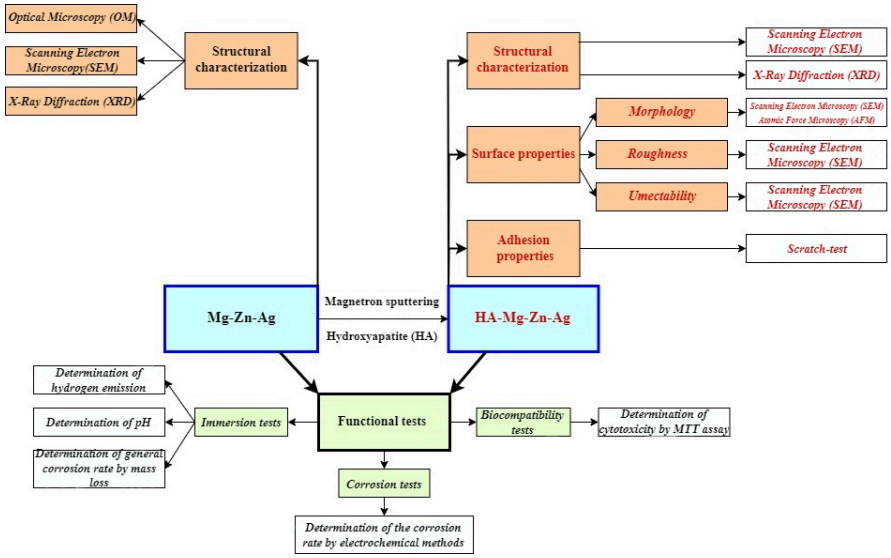


**Figure 3.1.** The working plan used

The experimental materials used in the doctoral thesis were:

- Magnesium alloys from the ternary system Mg-Zn-Ag, respectively ***Mg7Zn1Ag***: Zn – 7.1%, Ag – 1.5%, Mg – 91.4%; ***Mg6Zn3Ag***: Zn – 6.3%, Ag – 2.5%, Mg – 91.2%. These alloys were obtained from Dead Sea Magnesium Company (Beersheva, Israel). Magnesium was melted in a carbon steel melting pot, in a protective atmosphere of $CO_2$ + 0.5%$SF_6$. After the addition of 99.99% pure Zn and Ag elements into the melt, the melting pot was mechanically stirred for 5 minutes, then cooled directly in cold water, and the experimental samples were collected. The characterization, testing and demonstration of the functionality of magnesium alloys in the Mg-Zn-Ag system were carried out on metallographically prepared samples with the dimensions of 15 × 15 × 5 mm3 (width × length × height);
- Synthetic hydroxyapatite (HA) cathode target, $Ca_{10}(PO_4)_6(OH)_2$, purchased from Kurt J. Lesker, Germany. This was used in the coatings deposited by the magnetron sputtering method in the radio frequency mode. For the coating, magnesium alloy samples with dimensions of 15 × 15 × 5 $mm^3$, (width × length × height) were used. The hydroxyapatite-coated Mg7Zn1Ag alloy was coded ***HA-Mg7Zn1Ag***, and the hydroxyapatite-coated Mg6Zn3Ag alloy was coded ***HA-Mg6Zn3Ag***.

The synthetic description of the characterization methods and the equipment used for each of the experimental samples is presented in table 3.1.

**Table 3.1.** Characterization methods and equipment used

| **OBJECTIVE** | **METHOD** | | **EQUIPMENT** |
|---|---|---|---|
| | **Mg-Zn-Ag magnesium alloys** [samples code: Mg7Zn1Ag și Mg6Zn3Ag] | **Magnesium alloys coated with hydroxyapatite** [samples code: HA-Mg7Zn1Ag și HA-Mg6Zn3Ag] | |
| **Structural characterization** | Optical microscopy (MO) | - | Optical Microscope Olympus BX51 (Olympus Life and Materials Science Europa GMBH, Hamburg, Germaniy) |

| | | | |
|---|---|---|---|
| | Scanning electron microscopy (SEM) | - | Scanning electron microscope FEI QUANTA INSPECT F (FEI Company, Eindhoven, Netherlands) |
| | - | Fourier-transform infrared spectrometry (FTIR) | Spectrometer Jasco FT/IR 6300 (JASCO International Co., Tokyo, Japan) |
| | X-Ray Diffraction (XRD) | | Diffractometer Panalytical X-Pert PRO (Malvern, U.K.) |
| **Elemental composition** | Energy-dispersive X-ray spectroscopy (EDS) | | - EDS Spectrometer (FEI Company, Eindhoven, Netherlands)<br>- EDS Spectrometer (Bruker, Berlin Germany) |
| **Surface morphology** | - | Scanning electron microscopy (SEM)<br><br>Atomic force microscopy (AFM) | - Scanning electron microscope EDS-SEM-TM3030Plus (Bruker, Berlin, Germany)<br>- Atomic force microscope INNOVA VEECO (VEECO Instruments Inc., Cambridgeshire, UK) |
| **Wetting degree** | Contact angle (θ) | | System KRÜSS DSA30 Drop Shape Analysis (KRÜSS GmbH, Hamburg, Germany) |
| **Roughness surface** | - | Profilometry with electro-mechanical probe | Profilometer Dektak 150 (VEECO Instruments Inc., Cambridgeshire, UK) |
| **Adhesion properties** | - | Scratch test | Diamond penetrator type Rockwell |
| **Corrosion Resistance** | Hydrogen emission tests<br>Immersion tests<br><br>Electrochemical tests | | -<br>-<br>Potentiostat/Galvanostat Model PARSTAT 4000 (Princeton Applied Research, Oak Ridge, TN, USA) |

# CHAPTER 4. STRUCTURAL CHARACTERIZATION OF MAGNESIUM ALLOYS FROM THE Mg-Zn-Ag SYSTEM USABLE FOR ORTHOPEDIC IMPLANTS

## 4.1. Preparation of samples from experimental Mg-Zn-Ag alloys for metallographic examination

The metallographic examination of these alloys plays an important role in the microstructural characterization of these materials and the selection of the optimal alloy.

Cutting was done using the Delta Abrasimet Cutter, with a special abrasive disc for magnesium alloys, ensuring good cooling and a low cutting speed. The embedding of the samples was done cold in Epoxicure resin (Buehler GMBH product) because the use of hot

curing compounds that reach temperatures in excess of 150 ºC can cause structural changes that can lead to erroneous results.

Grinding was done with the Pheonix Alpha-Vector PowerHead. Grinding was performed with the help of metallographic papers (abrasive particles of silicon carbide) starting from abrasiveness 600 to 2400, under continuous jet and intermediate cooling with water. At the end of the operation, the samples were washed under running water to remove traces of abrasive or metal dust and wiped dry.

Polishing of the samples was done semi-automatically with the EcoMet 300 machine with a very low application force. The polished, mirror-like sample was washed with ethanol and dried in hot air.

The metallographic attack aims to highlight the structural constituents. The highlighting of the structure is achieved by attacking the surface with chemical reagents, generally acid solutions.

In the case of the experimental samples, the as-cast Mg7Zn1Ag and Mg6Zn3Ag alloys were chemically attacked with a solution consisting of 2.4 g of picric acid, 18 ml of glacial acetic acid, 76 ml of ethanol and 18 ml of distilled water, after which the samples were dried in hot air.

## 4.2. Microstructural characterization of Mg-Zn-Ag alloys

### 4.2.1. Optical microscopy determinations

The microstructures of the investigated alloys Mg7Zn1Ag and Mg6Zn3Ag are shown in Figures 4.1-4.2. Optical microscopy images reveal a specific casting structure for the magnesium-based alloys with polyhedral grains within which globular compounds are observed. Regarding the grain size, due to the higher silver content, the Mg6Zn3Ag alloy has smaller grain sizes.

Therefore, increasing the Ag content from 1.5% to 2.5% causes a refinement of the alloy structure (grain size reduction) and a more pronounced grain boundary due to the accumulation of Zn and Ag precipitates in this area.

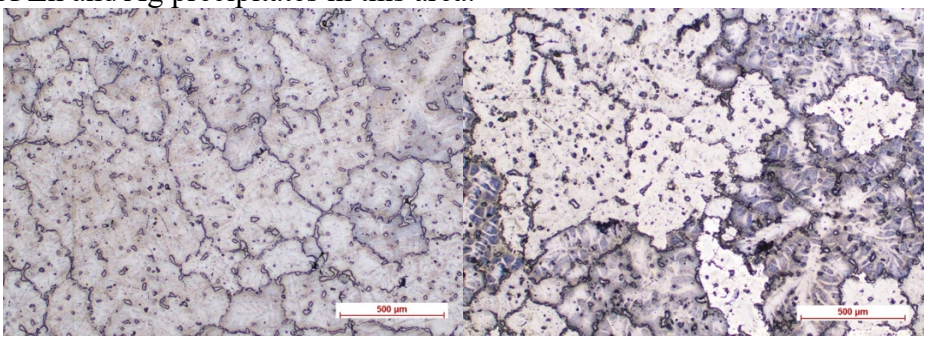


a) b)

**Figure 4.1.** Optical microscopy images – microstructure of Mg7Zn1Ag magnesium alloy, 5x magnification, on (a) unetched and (b) etched samples

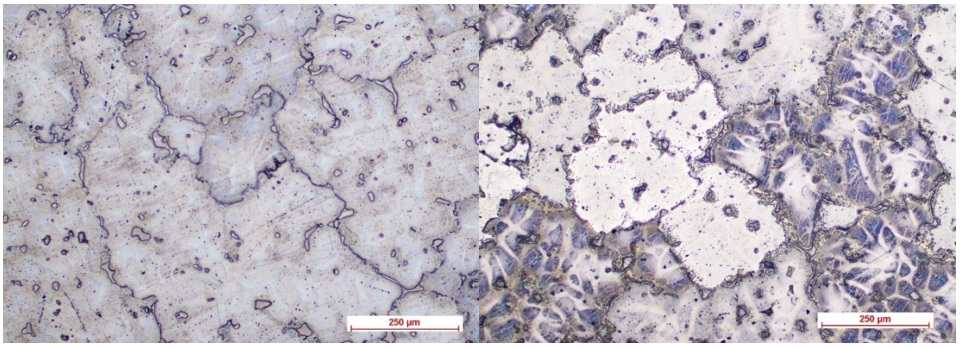


(a) (b)

**Figure 4.2**. Optical microscopy images – microstructure of Mg7Zn1Ag magnesium alloy, 10x magnification, on (a) unetched and (b) etched samples

4.2.2. Microstructural analysis by X-ray diffraction

The XRD diffraction patterns for the investigated alloys Mg7Zn1Ag, Mg6Zn3Ag are shown in Figure 4.5.

The structure of the magnesium alloys was revealed by identifying and indexing the diffraction peaks from the obtained X-ray diffractograms.

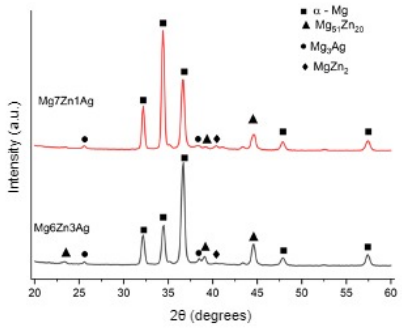


**Figure 4.5.** X-ray diffraction pattern for the experimental alloys in the Mg-Zn-Ag system

By increasing the Ag content from 1.5% to 2.5% (wt. %), a decrease in the intensity of the diffraction maximum corresponding to the compound MgZn2 is observed, while for the compounds $Mg_3Ag$ and $Mg_{51}Zn_{20}$, diffraction peaks of higher intensities are highlighted.

4.2.3. Microstructural and compositional characterization by scanning electron microscopy (SEM) coupled with EDX spectrometry

The results of the scanning microscopy (SEM) determinations are presented in Figures 4.6.-4.8. Relatively homogeneous structures are highlighted, the grain boundaries being clearly highlighted. SEM images of the Mg7Zn1Ag alloy (Figure 4.6.) highlight the morphology and distribution of the secondary phases ($MgZn_2$, $Mg_{51}Zn_{20}$ and $Mg_3Ag$).

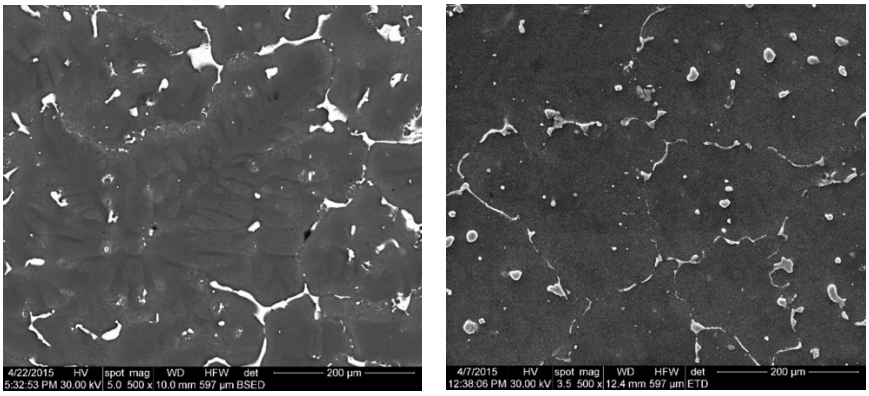


(a) (b)

**Figure 4.6.** The general aspect of the microstructure of the experimental alloys observed by scanning electron microscopy: a) Mg7Zn1Ag alloy; b) Mg6Zn3Ag alloy

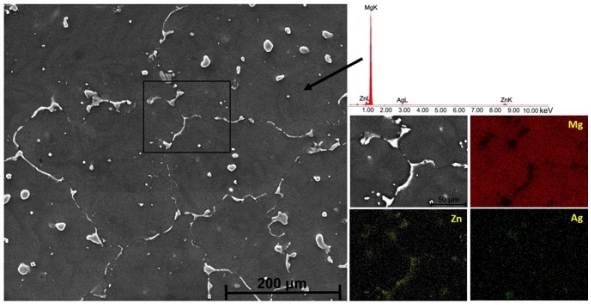


**Figure 4.7**. Results of scanning electron microscopy and EDS spectrometry determinations in the case of the Mg7Zn1Ag alloy

In order to determine the elemental composition of these compounds, scanning electron microscopy measurements coupled with EDS analyzes were performed (figures 4.7. and 4.8.).

For the Mg7Zn1Ag alloy the EDS images show that the $Mg_3Ag$ phase is mainly distributed in the globular compounds inside and at the grain boundary.

Also, the presence of compounds with Mg and Zn is observed at the grain boundary in both globular and lenticular compounds ($MgZn_2$, $Mg51Zn_{20}$).

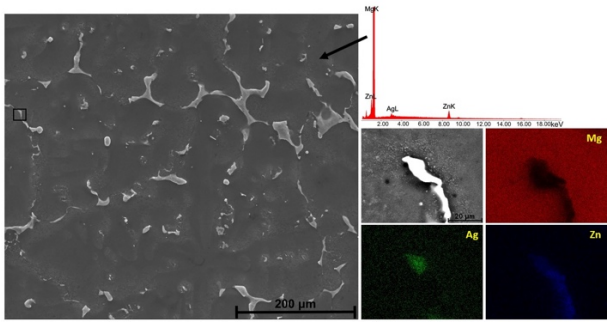


**Figure 4.8.** Results of scanning electron microscopy and EDS spectrometry determinations in the case of the Mg6Zn3Ag alloy

The Mg6Zn3Ag alloy (with a higher percentage of Ag) shows a similar morphology to the Mg7Zn1Ag alloy, but with a higher grain boundary density. The additional silver content was distributed both at the grain boundary ($Mg_3Ag$), thereby preventing grain growth, and within the grains. It can be said that the solubility of Ag in the magnesium matrix is increased, being detected in greater proportion inside the grains. Zn is mainly found in lenticular compounds, having also a low solubility inside the grains.

# CHAPTER 5. SURFACE MODIFICATION OF MAGNESIUM ALLOYS Mg-Zn-Ag THROUGH THE DEPOSITION OF HYDROXYAPATITE USING THE MAGNETRON SPUTTERING METHOD IN THE RADIO FREQUENCY MODE AND THEIR CHARACTERIZATION

## 5.1. Equipment used and experimental work protocol

Surface modification of Mg-Zn-Ag magnesium alloys was achieved by hydroxyapatite deposition using an OXI-AJA UHV radiofrequency magnetron sputtering system (AJA Int.). The installation consists of the following subassemblies:

- The technological enclosure (Figure 5.1.) consists of RF/DC magnetrons with pneumatically operated shutters and cathodes of diameter Φ = 1″; maximum working power of 100 W in DC and 100 W in RF;
- Support with rotation and heating of magnesium alloys at a constant temperature (room temperature ≅ 800°C). The support on which the magnesium alloy samples are placed is rotated by a DC motor powered by an external power source;
- The quartz microbalance is used to determine the deposition rate; this has as a sensor a disc-shaped quartz crystal;
- The vacuum system of the technological enclosure consists of a preliminary vacuum pump and a turbomolecular pump with magnetic levitation, which allow obtaining a minimum pressure of $1x10^{-7}$ mbar, the pressure in the enclosure being measured with the help of a vacuum meter system;
- The gas flow control system consists of three gas flow control transducers, with an adjustment range from 0 to 10 $cm^3$/min.;
- The control system for keeping the pressure constant during deposition, consisting of a drawer valve operated by a stepper motor and an electronic regulator that receives the error signal from the capacitive vacuum transducer;
- Sluice for introducing samples into the technological enclosure;
- The system of power sources, including power sources for the magnetrons and power sources for the support on which the magnesium alloy samples are placed;
- The command-and-control system of the deposition facility, which allows the control of all process parameters and their visualization during the deposition process (Figure 5.2.).

**Figure 5.1.** Technological enclosure

**Figure 5.2.** The command-and-control system of the deposition facility

The steps of the deposition process are briefly shown in Figure 5.3., and are the same regardless of the type of layer to be deposited.

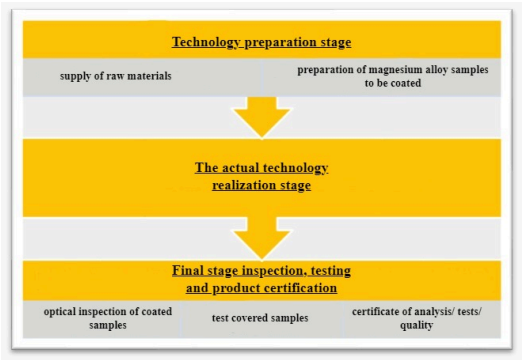


**Figure 5.3.** Technological stages of the substrate deposition process

Coating of Mg-Zn-Ag alloy samples with hydroxyapatite was performed by the RF magnetron sputtering method (13.56 MHz) using a hydroxyapatite cathode (1", 99.9% purity, Kurt J. Lesker Company).

The coatings were made using the following parameters:

- the RF feed power of the HA cathode target was kept constant at 50W;
- the pressure of argon (Ar) was 6.7 x $10^{-1}$ Pa;
- the base pressure in the deposition chamber was $1.3\times10^{-4}$ Pa,
- the bias voltage of the substrate was -60 V;
- the distance between the targets and the support on which the magnesium alloy samples are placed was 12 mm;
- the deposition time was 330 minutes.

The deposition temperature was maintained at 300°C to maintain the integrity of both magnesium alloys. It is well known that up to 400°C, the Mg-based alloy did not undergo changes [184–186]. The thickness of the coatings obtained was approximately 400 nm.

The hydroxyapatite-coated Mg7Zn1Ag alloy was coded ***HA-Mg7Zn1Ag***, and the hydroxyapatite-coated Mg6Zn3Ag alloy was coded ***HA-Mg6Zn3Ag***.

## 5.2. Characterization of the deposited hydroxyapatite layer

5.2.1. Structural characterization of the deposited layer

In order to highlight the phase composition of the HA layers obtained at 300°C on the magnesium alloy samples, Mg7Zn1Ag and Mg6Zn3Ag, XRD analyses were performed at grazing angles. In the case of deposited hydroxyapatite layers, the intensities related to the phases in the magnesium alloys are very intense and thus those of the layer are masked (figure 5.4.). For example, the diffraction peak located at 32.20° can be assigned to both α-Mg and HA phases.

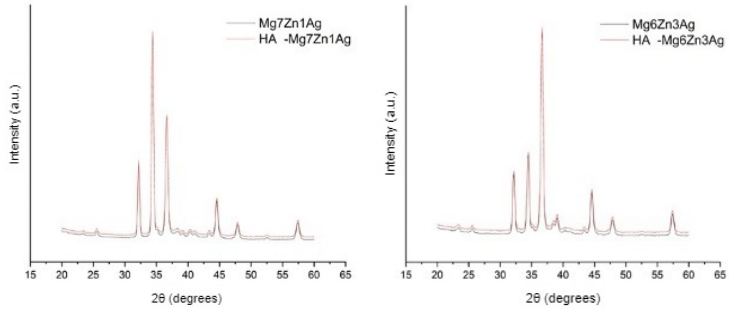


**Figure 5.4.** XRD diffractograms for Mg–Zn–Ag alloys and Mg–Zn–Ag alloys coated with HA

To show that the deposited layer is one based on calcium phosphate, an artifice was used: a Si substrate was introduced into the deposition chamber and covered with HA together

with the magnesium alloy samples. Thus, the XRD analyses were no longer influenced by the information captured from the two magnesium alloy samples.

Figure 5.5 shows the diffractogram of HA layers deposited at 300°C on a Si substrate. It is noteworthy that hydroxyapatite (HA) phases were obtained even at a temperature of 300°C (assignment of diffraction peaks was performed according to JCPDS No. 09–0432).

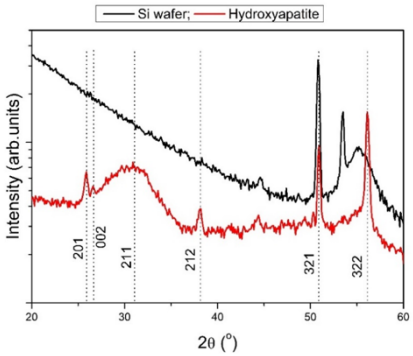


**Figure 5.5.** Diffractogram of the deposited hydroxyapatite layer

FTIR evaluation was performed on the coating deposited on the Si plate to demonstrate that there is HA on the surface of the samples.

As shown in Figure 5.6, the IR transmission spectra of the hydroxyapatite coating revealed specific bands corresponding to phosphate functional groups. Strong absorption bands between 500 and 1100 $cm^{-1}$ indicated the presence of two vibrational modes of phosphate ions, ν3 and ν4.

The intense band from 1026 $cm^{-1}$ was assigned to the asymmetric stretching vibration of the $PO_4^{3-}$ group (ν3), and the bands from 565 and 615 $cm^{-1}$ were assigned to the asymmetric bending vibrations (ν4) of the $PO_4^{3-}$ group.

In the interval 1680 and 1400 $cm^{-1}$ low intensity bands attributed to the carbonate group ($CO_3^{2-}$) were identified.

The bands corresponding to the $OH^{-1}$ group are clearly observed between 3000 and 3700 $cm^{-1}$ and could be associated with water molecules adsorbed on the sample surface.

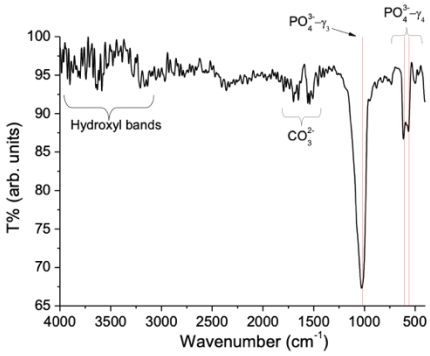


**Figure 5.6.** FTIR spectra of the deposited hydroxyapatite layer

5.2.2. Determination of surface properties

***<u>Determination of surface properties by SEM-EDS</u>***

Figures 5.7. and 5.8. shows the SEM images and EDS spectra of samples Mg-Zn-Ag alloys and coated Mg-Zn-Ag alloys. SEM micrographs were analysed to evaluate the surface morphology of the Mg-Zn-Ag alloy samples, as well as the homogeneity and uniformity of the HA coatings.

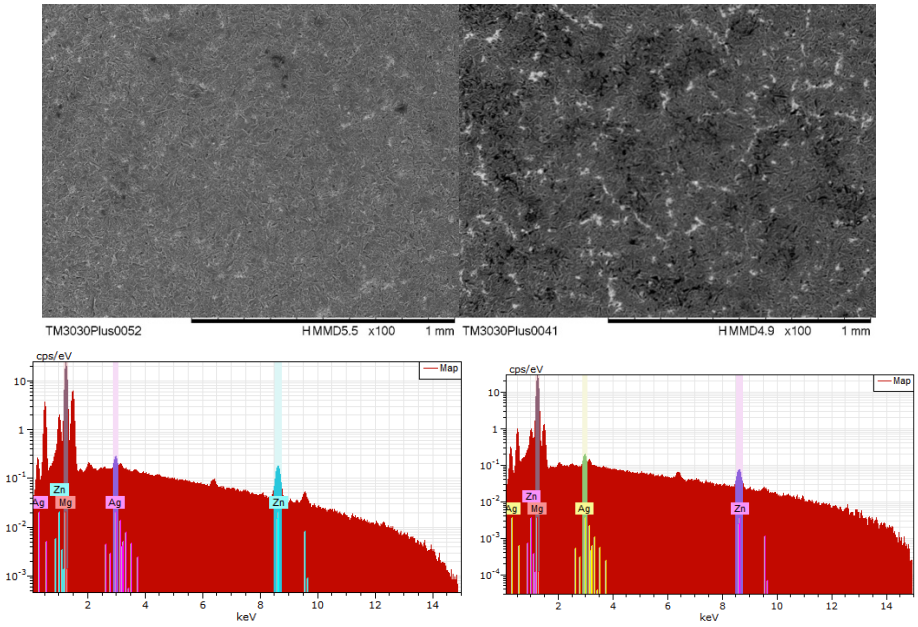


(a) (b)

**Figure 5.7.** SEM images and EDS spectra of samples of: (a) Mg7Zn1Ag alloy and (b) Mg6Zn3Ag alloy

As can be seen, the hydroxyapatite layers deposited on the surface of the magnesium alloy samples (Mg7Zn1Ag, Mg6Zn3Ag) are very thin, which allows the visualization of grain boundaries, especially in the case of the HA-Mg6Zn3Ag sample, where they are better defined. However, the HA coatings are homogeneously deposited on the surface of both magnesium alloy samples without cracks or other visible defects.

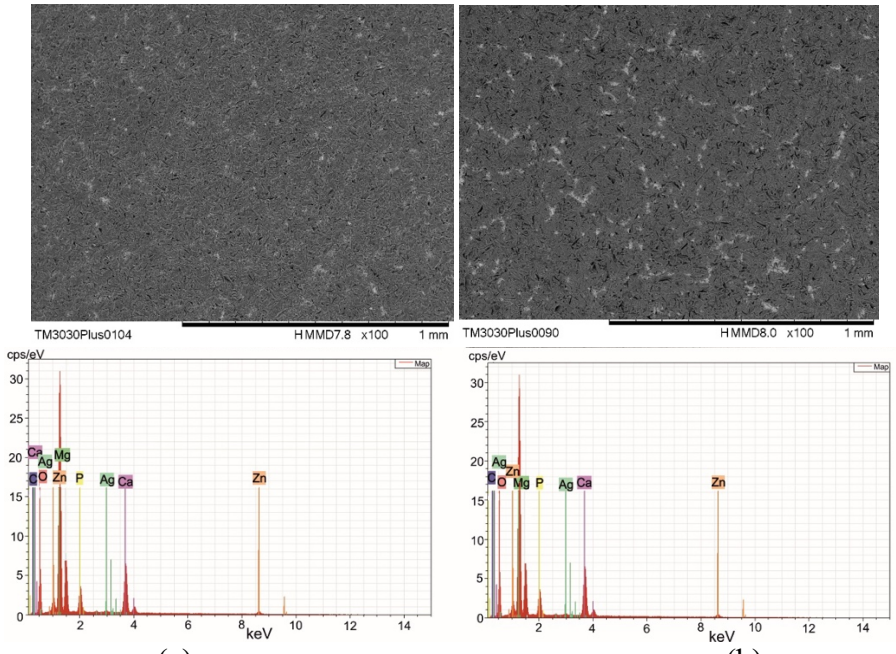


(a) (b)

**Figure 5.8.** SEM images and EDS spectra of (a) HA-Mg7Zn1Ag and (b) HA-Mg6Zn3Ag samples

In Table 5.1. the elemental composition of the coatings deposited on the surface of the Mg-Zn-Ag alloy samples is presented. It can be seen that in the case of the HA-Mg7Zn1Ag

sample, the Ca/P ratio is equal to 1.71, while for the HA-Mg6Zn3Ag sample, this ratio is approximately 1.69, highlighting the achievement of stoichiometric hydroxyapatite coatings in both cases. So, the deposition temperature of 300°C is sufficient to obtain a crystalline hydroxyapatite structure.

**Table 5.1.** Elemental composition of HA coated magnesium alloy samples

| Sample | Mg (% at.) | Ca (% at.) | P (% at.) | Zn (% at.) | Ag (% at.) | O (% at.) |
|---|---|---|---|---|---|---|
| HA-Mg7Zn1Ag | 51,2 | 15,8 | 9,2 | 1,1 | 0,2 | 22,5 |
| HA-Mg6Zn3Ag | 55,5 | 12,9 | 7,6 | 5,1 | 0,5 | 18,4 |

***Determination of surface properties by AFM***

The topography of the coated Mg-Zn-Ag alloy samples is presented in Figures 5.11. and 5.12. It can be seen that there are no major differences in the surface area of the hydroxyapatite coating regardless of the type of Mg-Zn-Ag magnesium alloy on which the deposition was performed.

This fact is not surprising, since all the experimental samples of Mg-Zn-Ag magnesium alloys on which the depositions were carried out presented surfaces with an identical roughness after the polishing process.

Analysis of the coated samples revealed a number of fine particles on both coated surfaces, indicating that fine-structured hydroxyapatite coatings were obtained. The atomic force microscopy results confirm and support the conclusions drawn from the scanning electron microscopy investigations.

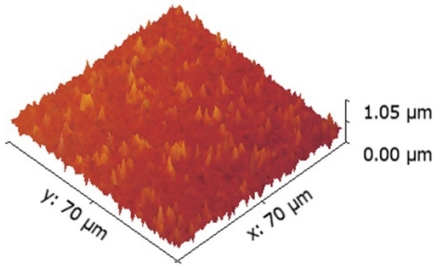


**Figure 5.11**. 3D AFM image for the HA-Mg7Zn1Ag sample

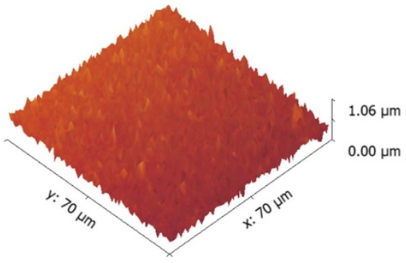


**Figure 5.12.** 3D AFM image for the HA-Mg6Zn3Ag sample

***Determination of roughness***

In general, surface roughness is a critical parameter that is directly related to the integration of an implant into the human body.

Considering the Ra parameter, the surface roughness is 1146.76 nm for the HA-Mg6Zn3Ag sample and 1035.50 nm for the HA-Mg7Zn1Ag sample, respectively (Table 5.2.).

**Table 5.2.** Roughness parameters of Mg-Zn-Ag alloys coated with hydroxyapatite

| Sample | $R_a$ (nm) | $R_{sk}$ |
|---|---|---|
| HA-Mg7Zn1Ag | 1035,50 | 0,12 |
| HA- Mg6Zn3Ag | 1146,76 | 0,04 |

The HA-Mg6Zn3Ag sample shows a lower asymmetry parameter value (0.04) being closer to 0, which means that the surfaces are closer to a flat surface.

It can be seen that the values obtained for $R_a$ and $R_{sk}$ can be correlated as follows, an $R_{sk}$ value close to zero means an equal distribution of valleys and peaks, and an increased value of the $R_a$ parameter characterizes a large area.

Figures 5.13 and 5.14 show the 3D SEM images of the HA-Mg7Zn1Ag and HA-Mg6Zn3Ag samples that highlight the surface roughness.

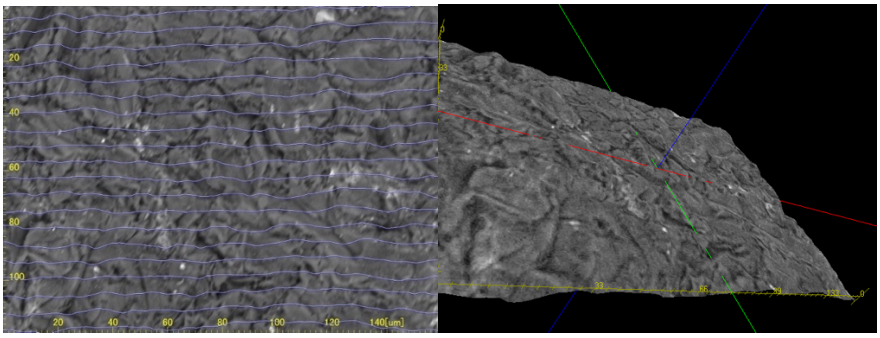

**Figure 5.13.** 3D SEM images of the HA-Mg7Zn1Ag sample highlighting the surface roughness

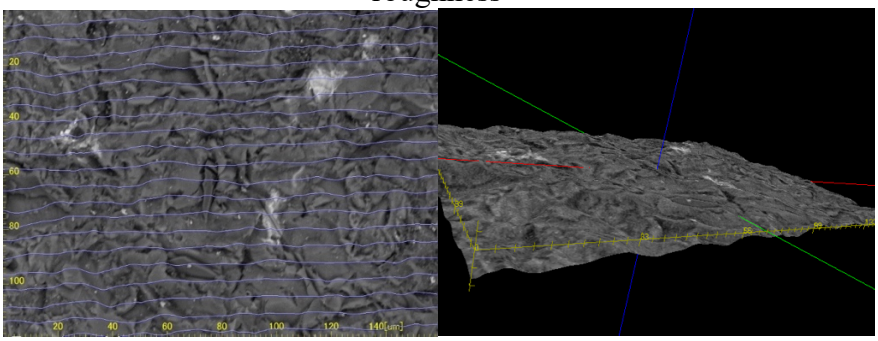

**Figure 5.14.** 3D SEM images of the HA-Mg6Zn3Ag sample highlighting the surface roughness

***Determination of wettability by the contact angle method***

The values obtained for all investigated samples are presented in Table 5.3. Magnesium alloys Mg7Zn1Ag and Mg6Zn3Ag show a high contact angle with a tendency towards a hydrophobic surface. It can be seen that the application of a hydroxyapatite coating caused a decrease in the hydrophobicity of the magnesium alloys and lower values of the contact angles in the range of 72-75° were obtained.

**Table 5.3.** The values of the contact angle of the experimental samples

| Sample | Contact angle (°) |
|---|---|
| HA-Mg7Zn1Ag | 74,71 ± 2,56 |
| HA-Mg6Zn3Ag | 72,23 ± 3,08 |
| Mg7Zn1Ag | 85,54 ± 2,21 |
| Mg6Zn3Ag | 81,72 ± 2,16 |

The images with the appearance of the water droplets deposited on the surface of the investigated samples are presented in figure 5.15.

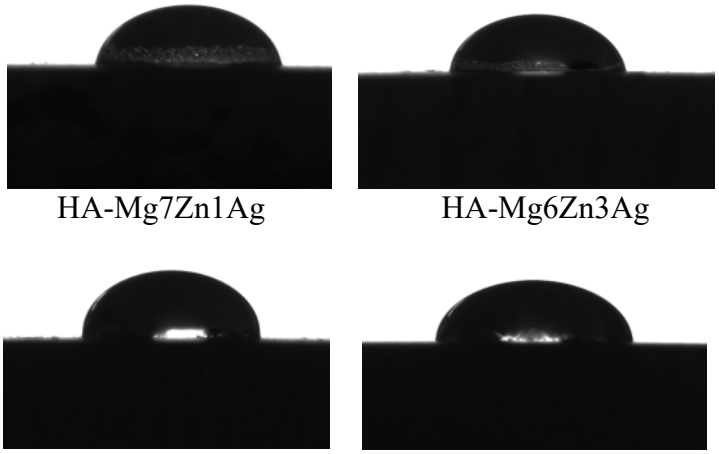

HA-Mg7Zn1Ag HA-Mg6Zn3Ag

Mg7Zn1Ag Mg6Zn3Ag

**Figure 5.15.** Comparative contact angle images of magnesium alloys and hydroxyapatite films obtained by RF-MS

5.2.3. Determination of adhesion properties by the scratch-test method

Figures 5.16. and 5.17. shows the scratch marks obtained during the scratch test on both HA-coated magnesium alloys.

The scanning electron microscopy images obtained on the experimental samples after testing are relatively similar, indicating that the nature of the magnesium alloy does not influence the adhesion of the coatings to it.

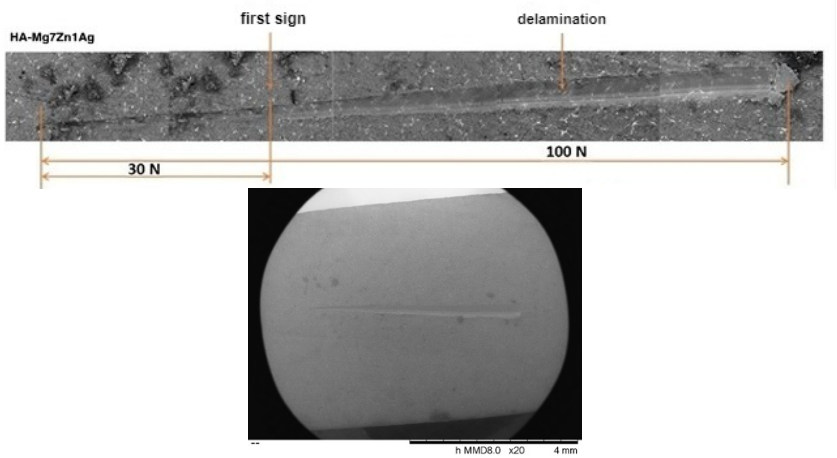


**Figure 5.16.** Scratch marks and critical load at first sign of coating delamination for HA-Mg7Zn1Ag samples

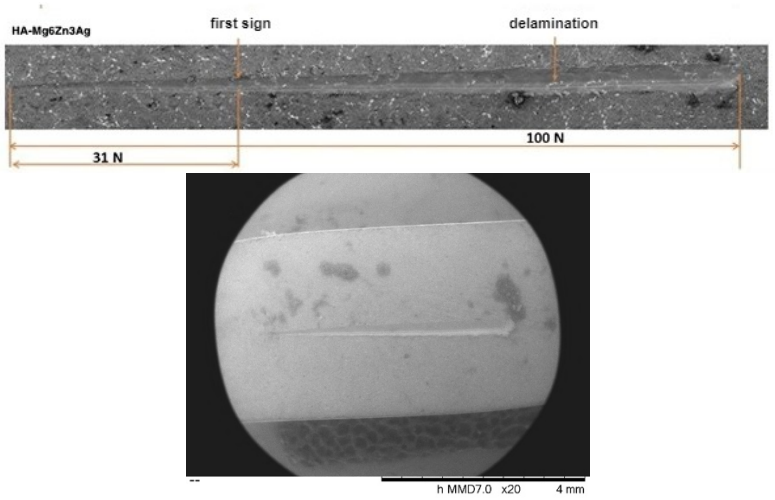


**Figure 5.17.** Scratch marks and critical load at first sign of coating delamination for HA-Mg6Zn3Ag samples

# CHAPTER 6. FUNCTIONAL TESTING OF MAGNESIUM ALLOYS Mg-Zn-Ag

## 6.1. Determination of corrosion resistance in simulated environments of experimental Mg-Zn-Ag magnesium alloys, before and after coating with hydroxyapatite

The corrosion behaviour of biodegradable magnesium alloys with Ag incorporated is mainly governed by the following three factors:

(1) weight and distribution of Ag-containing secondary phases; these phases can act as a cathode and accelerate micro-galvanic corrosion;

(2) the presence of Ag as a solute in the magnesium matrix; increases corrosion resistance by improving the standard electrode potential of the alloy;

(3) grain size.

### 6.1.1. Determination of corrosion resistance by electrochemical methods

Corrosion resistance tests for Mg7Zn1Ag and Mg6Zn3Ag alloys were performed in the following media simulating biological fluids: simulated body fluid (SBF) solution and Dulbecco's Modified Eagle's Medium (DMEM).

Tafel curves corresponding to Mg7Zn1Ag and Mg6Zn3Ag alloys recorded in the test media (DMEM and SBF) are shown in Figures 6.1. and 6.2.

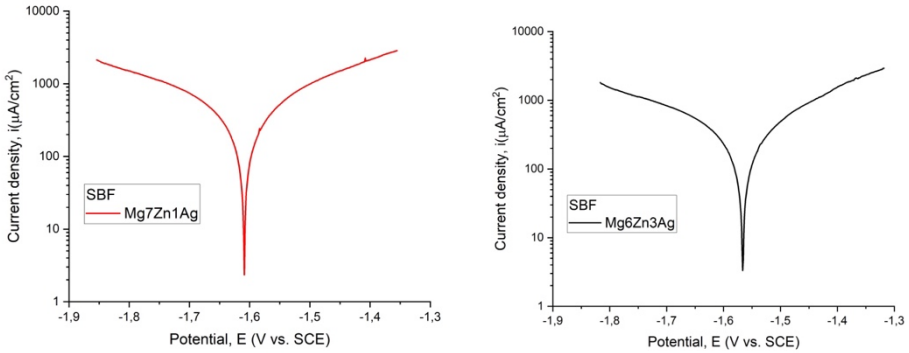


**Figure 6.1.** Tafel curves of Mg7Zn1Ag and Mg6Zn3Ag alloys, after immersion in SBF

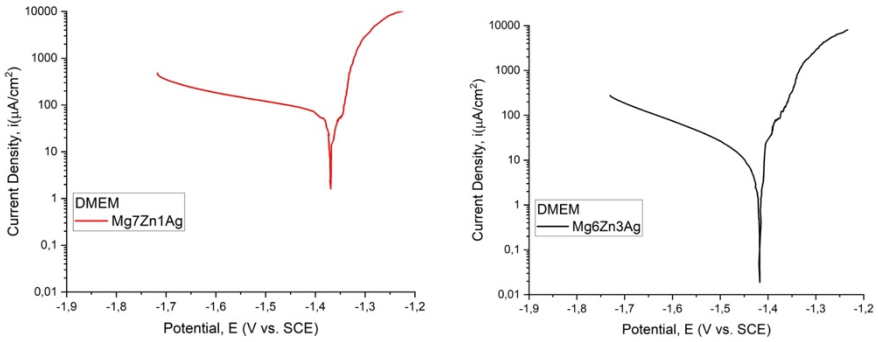


**Figure 6.2.** Tafel curves of Mg7Zn1Ag and Mg6Zn3Ag alloys, after immersion in DMEM

To highlight more clearly the evolution of the Tafel curves, they were overlapped, thus obtaining a graph for each test environment used (Figures 6.3 - 6.4.).

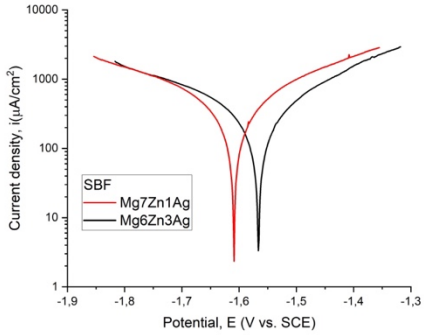


**Figure 6.3**. Tafel curves of Mg-Zn-Ag alloys after immersion in SBF

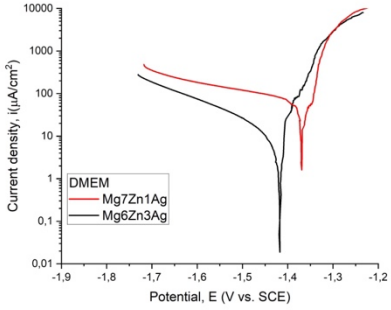


**Figure 6.4.** Tafel curves of Mg-Zn-Ag alloys after immersion in DMEM

The results obtained on the investigated Mg-Zn-Ag alloys are presented in Table 6.1. and Table 6.2.

**Table 6.1.** Main electrochemical parameters in SBF

| Alloy | $E_{oc}$ (V) | $E_{corr}$ (V) | $i_{corr}$ (μA/cm²) | CR (mm/an) | $\beta_c$ (mV) | $\beta_a$ (mV) | $R_p$ (kΩcm²) |
|---|---|---|---|---|---|---|---|
| Mg6Zn3Ag | -1,569 | -1,566 | 990,876 | 22,014 | 901,242 | 517,542 | 0,144 |
| Mg7Zn1Ag | -1,606 | -1,609 | 1345,000 | 28,834 | 902,334 | 619,550 | 0,118 |

**Table 6.2.** Main electrochemical parameters in DMEM

| Alloy | $E_{oc}$ (V) | $E_{corr}$ (V) | $i_{corr}$ (μA/cm$^2$) | CR (mm/an) | $\beta_c$ (mV) | $\beta_a$ (mV) | $R_p$ (kΩcm$^2$) |
|---|---|---|---|---|---|---|---|
| Mg6Zn3Ag | -1,455 | -1,386 | 8,081 | 0,173 | 207,900 | 115,857 | 3,573 |
| Mg7Zn1Ag | -1,476 | -1,401 | 9,053 | 0,201 | 252,470 | 51,531 | 2,302 |

In terms of corrosion current density and corrosion rate in both test environments, the corrosion resistance of the alloys decreases as follows: Mg6Zn3Ag, Mg7Zn1Ag.
The Mg6Zn3Ag and Mg7Zn1Ag alloys are silver-containing materials (2.5 wt.% and 1.5 wt.%, respectively). It was observed that when the percentage of Ag increases, the $Mg_3Ag$ and $Mg_{51}Zn_{20}$ phases are more pronounced and the $MgZn_2$ phase is significantly reduced [208].

In our case, the Mg6Zn3Ag alloy with a higher percentage of silver (2.5 wt. %) showed better corrosion resistance (SBF - Rp = 0.144 kΩcm$^2$, CR = 22.014 mm/year and DMEM - Rp = 3.573 kΩcm$^2$, CR = 0.173 mm/year) than Mg-7Zn-1Ag (SBF - Rp = 0.118 kΩcm$^2$, CR = 28.834 mm/year and DMEM - Rp = 2.302 kΩcm2, CR = 0.201 mm/year). The higher Ag content results in a more refined structure that results in increased corrosion resistance. Also some of the excess silver is distributed as a solute in the magnesium matrix and increases the corrosion resistance by improving the standard electrode potential of the alloy.

For the determination of corrosion resistance on magnesium alloys coated with hydroxyapatite (HA-Mg7Zn1Ag and HA-Mg6Zn3Ag) simulated body fluid (SBF) solution was used as the test medium.

The variations of the open circuit potential ($E_{oc}$) corresponding to the coatings are shown in Figure 6.5., and the Tafel curves are shown in Figure 6.6.

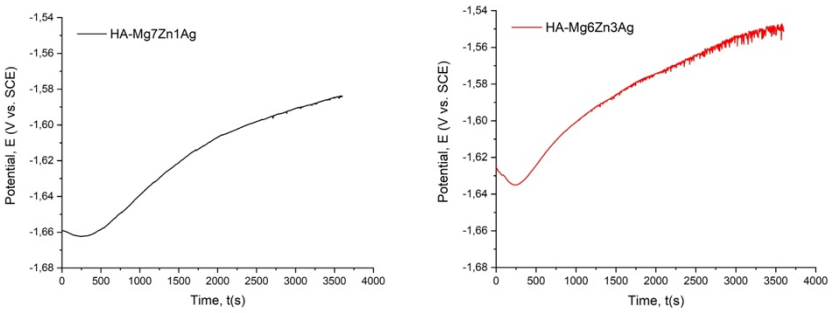


**Figure 6.5.** Variation of open circuit potential for HA-Mg7Zn1Ag and HA-Mg6Zn3Ag samples after immersion in SBF

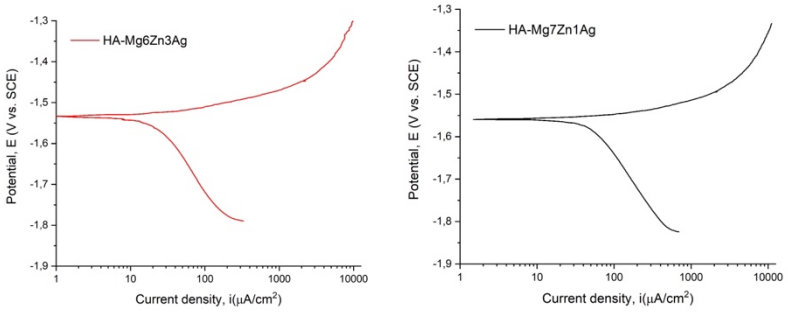


**Figure 6.6.** Tafel curves of HA-Mg7Zn1Ag and HA-Mg6Zn3Ag samples after immersion in SBF

Considering the values of open circuit potential ($E_{oc}$) and corrosion potential ($E_{corr}$) it is known that their more electropositive values characterize a higher corrosion resistance of

the material [247, 248]. Electrochemical measurements show that the highest values of $E_{oc}$ and $E_{corr}$ are obtained for the sample HA-Mg6Zn3Ag (Table 6.3.).

**Table 6.3.** Main electrochemical parameters in SBF

| Sample | $E_{oc}$ (V) | $E_{corr}$ (V) | $i_{corr}$ ($\mu A/cm^2$) | $\beta_c$ (mV) | $\beta_a$ (mV) | $R_p$ ($k\Omega cm^2$) | $P_e$ (%) | CR (mm/year) |
|---|---|---|---|---|---|---|---|---|
| HA-Mg7Zn1Ag | -1,583 | -1,559 | 57,470 | 345,100 | 35,510 | 0,243 | 95,720 | - |
| HA-Mg6Zn3Ag | -1,550 | -1,533 | 25,850 | 366,170 | 44,720 | 0,670 | 97,390 | - |
| Mg6Zn3Ag | -1,569 | -1,566 | 990,876 | 901,242 | 517,542 | 0,144 | - | 22,014 |
| Mg7Zn1Ag | -1,606 | -1,609 | 1345,000 | 902,334 | 619,550 | 0,118 | - | 28,834 |

It was observed that the Mg-Zn-Ag samples coated with HA had lower corrosion current density values, which highlighted the beneficial effect of the coating against the corrosion phenomenon. The lowest value of this parameter (25.85 $\mu A/cm^2$) was recorded for the HA-Mg6Zn3Ag sample, followed by the HA-Mg7Zn1Ag sample, which presented a value equal to 57.47 $\mu A/cm^2$. Based on the electrochemical parameters shown in Table 6.3, considering the $P_e$ protection efficiency, it can be seen that HA-Mg6Zn3Ag has a higher value than HA-Mg7Zn1Ag, a remark that can be correlated with better corrosion resistance. The corrosion rate CR is a parameter that can only be calculated for uncoated samples. A higher CR value is obtained for the Mg6Zn3Ag alloy, which exhibits better corrosion behaviour due to the addition of a larger amount of silver in its composition.

6.1.2. Determination of resistance to generalized corrosion by immersion tests

***Determination of the amount of hydrogen released in simulated environments***

In figures 6.9. - 6.11. the evolution of hydrogen release rate and pH on uncoated and HA-coated Mg7Zn1Ag and Mg6Zn3Ag alloys during immersion in SBF medium for 10 days are shown.

It can be seen from the figures that the average values of the hydrogen release rate between the uncoated and coated Mg7Zn1Ag and Mg6Zn3Ag alloys are substantially different during the SBF immersion process.

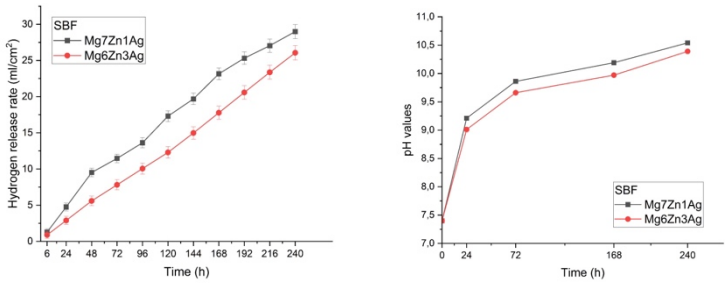


**Figure 6.9**. Evolution of hydrogen release rate and pH, in SBF solution, for Mg-Zn-Ag magnesium alloys

Compared to the uncoated alloys, the hydrogen release rate for the HA-coated alloys is lower and after 24 hours reaches substantially lower values (HA-Mg7Zn1Ag - 0.75 $ml/cm^2$ at pH=8.58; HA -Mg6Zn3Ag - 0.47 $ml/cm^2$ at pH=8.35).

The pH evolution over time reveals a stronger alkalinization of the medium for the uncoated magnesium samples than for the HA-coated magnesium samples. And through this

analysis, a more intense corrosion process is highlighted for the samples from uncoated magnesium alloys, Mg7Zn1Ag and Mg6Zn3Ag.

In the case of HA-coated alloys the pH of the test medium begins to stabilize after 168 hours (7 days) due to stable corrosion products (apatites) forming on the surface of the samples and providing additional protection against the corrosive environment.

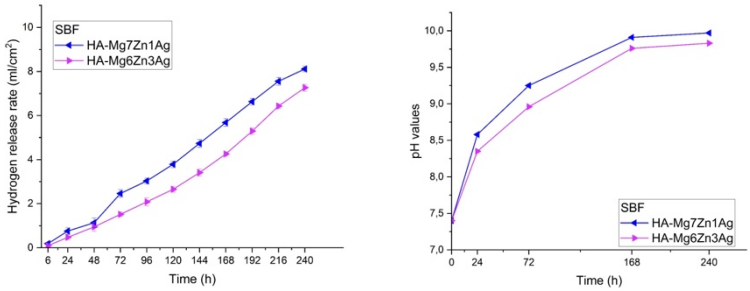


**Figure 6.10**. Evolution of hydrogen release rate and pH, in SBF solution, for HA-coated Mg-Zn-Ag alloys

From figure 6.12. it can be seen that for both HA-coated magnesium alloys the hydrogen release rates per day are between 0.56 ml/cm$^2$/day and 0.95 ml/cm$^2$/day for HA-Mg7Zn1Ag and 0.47 ml/cm2 /day and 0.83 ml/cm2/day in the case of the HA-Mg6Zn3Ag sample. These values are lower than the maximum limit tolerated by the human body of 2.25 ml/cm$^2$/day.

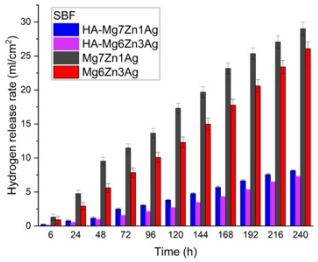


**Figure 6.11.** Evolution of hydrogen release rate, in SBF medium, for uncoated and HA-coated Mg-Zn-Ag alloys

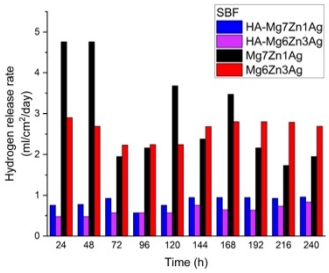


**Figure 6.12.** Evolution of hydrogen release rate per day, in SBF environment, for uncoated and HA-coated Mg-Zn-Ag alloys

The best corrosion behaviour evaluated by determining the hydrogen release rate in the SBF medium is the alloy with higher silver content coated with HA, HA-Mg6Zn3Ag, the release rate after 10 days of immersion being 6.26 ml/cm$^2$, and the hydrogen release rate per day of 0.83 ml/cm$^2$/day.

The evolution of the hydrogen release rate and the pH using Dulbecco's Modified Eagle's Medium (DMEM) solution as a test medium are shown in Figures 6.13-6.15.

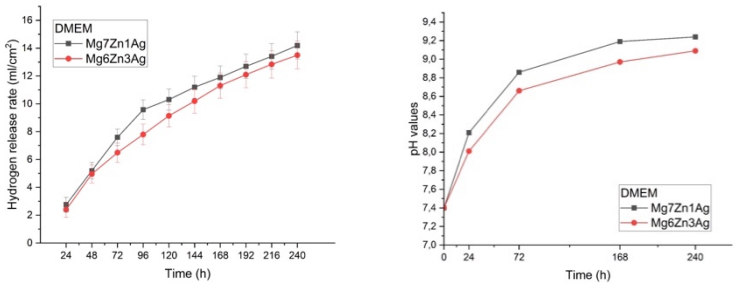


**Figure 6.13.** Evolution of hydrogen release rate and pH, in DMEM medium, for Mg-Zn-Ag alloys

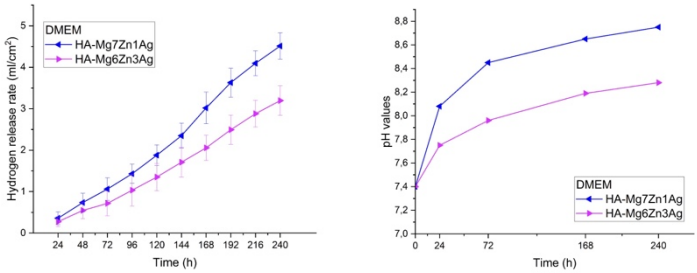


**Figure 6.14.** Evolution of hydrogen release rate and pH, in DMEM medium, for Mg-Zn-Ag alloys coated with HA

The hydrogen release rate values obtained using the DMEM solution as the test medium are superior to those obtained in the SBF solution, especially for the uncoated magnesium alloys.

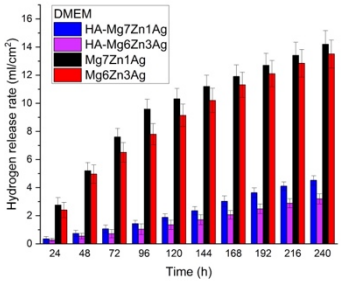


**Figure 6.15.** Evolution of hydrogen release rate, in DMEM medium, for uncoated and HA-coated Mg-Zn-Ag alloys

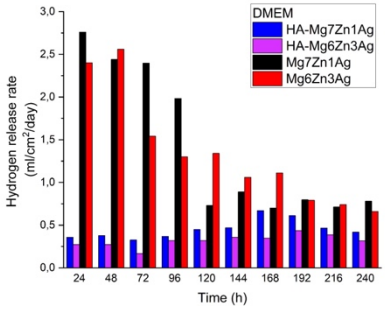


**Figure 6.16.** Evolution of hydrogen release rate per day, in DMEM medium, for uncoated and HA-coated Mg-Zn-Ag alloys

The hydroxyapatite-coated magnesium alloys behave similarly to the SBF medium, with a maximum hydrogen release rate per day of 0.66 ml/cm$^2$/day for HA-Mg7Zn1Ag and 0.43 ml/cm$^2$/day for HA-Mg6Zn3Ag.

***Determination of corrosion rate and mass loss by immersion tests in simulated environments***

The results of corrosion tests performed by immersing the experimental coated and uncoated Mg-Zn-Ag alloys in SBF and DMEM media for 72, 168 and 240 hours, respectively, are presented in Figures 6.17-6.21.

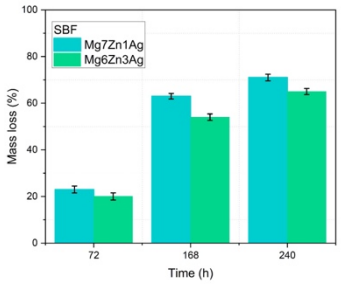


**Figure 6.17.** Mass loss evolution of Mg-Zn-Ag alloys in SBF

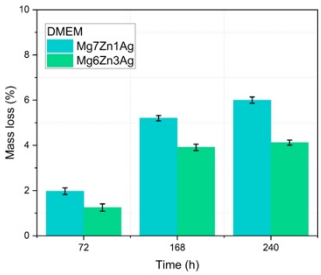


**Figure 6.18.** Evolution of mass loss of Mg-Zn-Ag alloys in DMEM

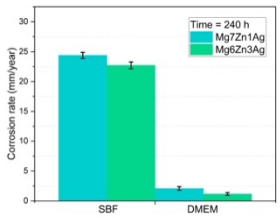


**Figure 6.19.** Corrosion rate of Mg-Zn-Ag alloys, after 240 hours of immersion in SBF and DMEM media

It is observed that the lowest mass loss was obtained for the Mg6Zn3Ag alloy in both media simulating the biological fluids used (65% at 240 hours in SBF and 4.12% at 240 hours in DMEM). The higher Ag content in the Mg6Zn3Ag alloy compared to the Mg7Zn1Ag alloy induces lower mass loss and a lower corrosion rate.

For the HA-coated Mg-Zn-Ag alloys, the results of corrosion tests performed by immersing them in SBF and DMEM media are shown in Figures 6.20. and 6.21.

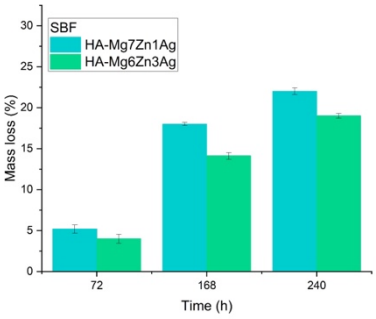

**Figure 6.20.** Mass loss evolution of HA-coated Mg-Zn-Ag alloys in SBF

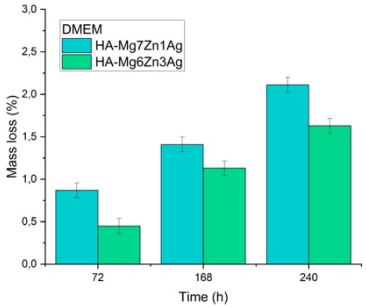


**Figure 6.21.** Evolution of mass loss of HA-coated Mg-Zn-Ag alloys in DMEM

It can be seen that the lowest mass loss was obtained for the HA-Mg6Zn3Ag sample in both test media used (19% at 240 hours in SBF media and 1.63% at 240 hours in DMEM media). Figures 6.22.-6.29 show the SEM images illustrating the surface of the samples from the experimental alloys Mg7Zn1Ag and Mg6Zn3Ag after 10 days of immersion in SBF and DMEM media. The SEM image on the Mg7Zn1Ag alloy after 10 days of immersion in the SBF solution, highlights the formation of a layer of corrosion products with a large number of clusters on the surface (Figure 6.22.). The presence of this layer suggests that the processes on the surface of the alloy proceed quickly, but without the formation of cracks that could produce an aggressive corrosion process.

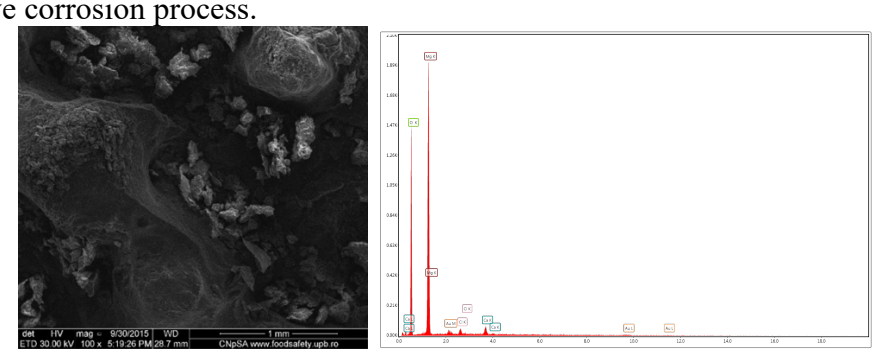

**Figure 6.22.** SEM-EDX experimental results on the surface of the Mg7Zn1Ag alloy following the determination of corrosion resistance by immersion tests in SBF after 10 days, before the removal of corrosion

The SEM image of the alloy after the removal of the corrosion products (Figure 6.23.) highlights the type of corrosion of magnesium alloys, namely pitting corrosion.

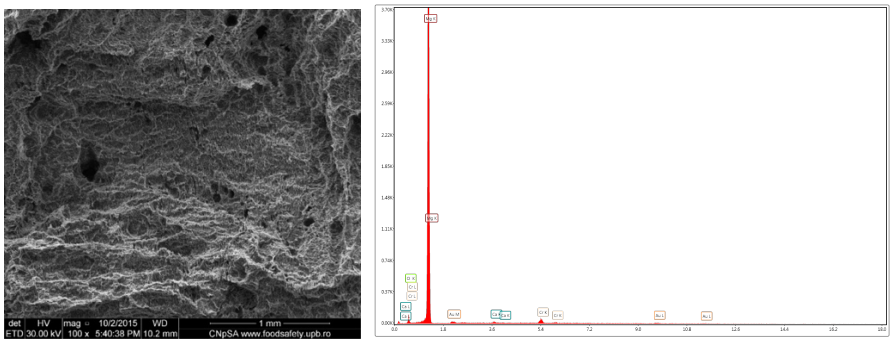

**Figure 6.23.** SEM-EDX experimental results on the surface of the Mg7Zn1Ag alloy following the determination of corrosion resistance by immersion tests in SBF after 10 days, after the removal of corrosion products

For Mg6Zn3Ag alloy (Figure 6.24. and 6.25.) the corrosion process proceeds similarly but with a lower intensity. The EDS spectra indicate the presence of the elements Mg, O and Cl, i.e. the formation of magnesium hydroxide layer ($Mg(OH)_2$) and magnesium chloride ($MgCl_2$).

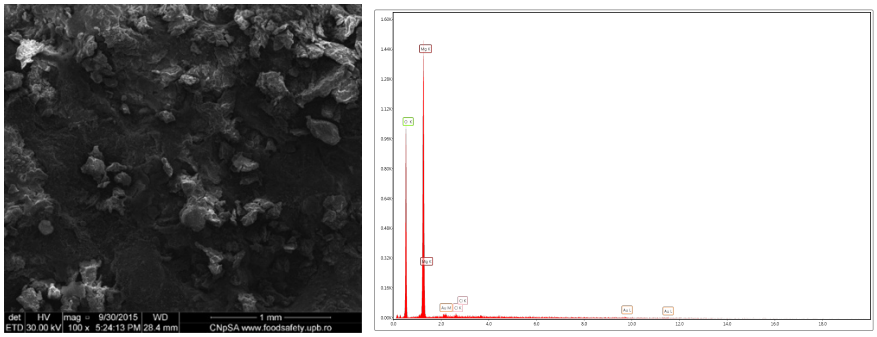

**Figure 6.24.** SEM-EDX experimental results on the surface of the Mg6Zn3Ag alloy following the determination of corrosion resistance by immersion tests in SBF after 10 days, before the removal of corrosion products

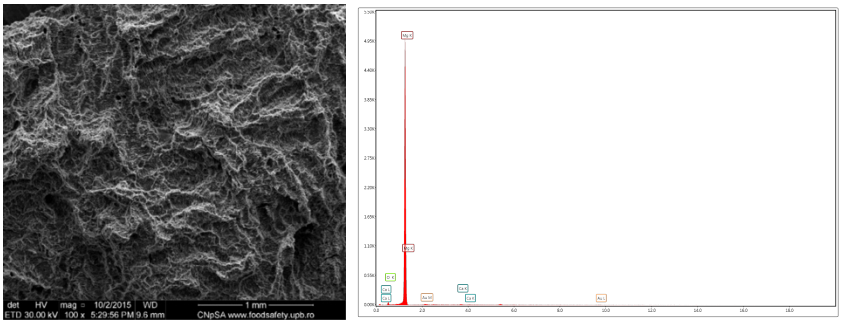

**Figure 6.25.** SEM-EDX experimental results on the surface of the Mg6Zn3Ag alloy following the determination of corrosion resistance by immersion tests in SBF after 10 days, after the removal of corrosion products

SEM images and EDS spectra on magnesium alloys investigated using DMEM solution as test medium indicate the formation of corrosion products $Mg(OH)_2$ and $MgCl_2$ on the surface of the alloy, as well as the formation of apatites.

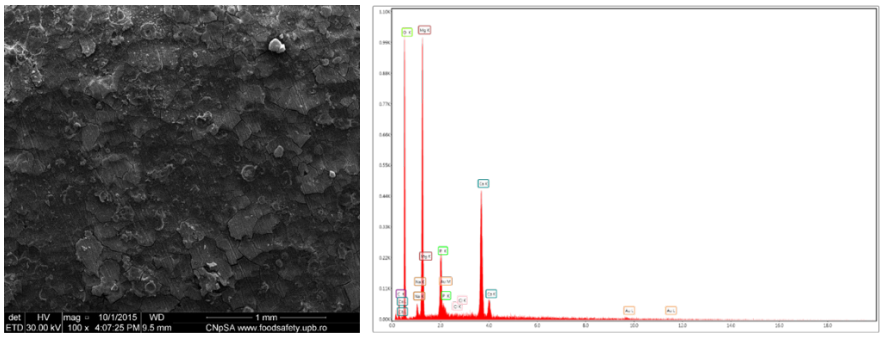

**Figure 6.26.** SEM-EDX experimental results on the surface of the Mg7Zn1Ag alloy following the determination of corrosion resistance by immersion tests in DMEM after 10 days, before the removal of corrosion products

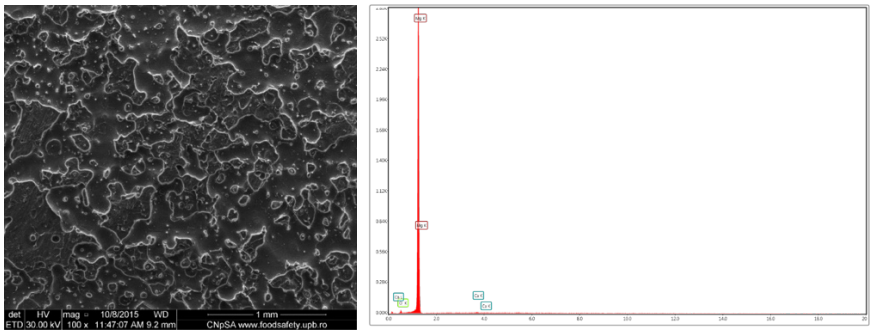

**Figure 6.27.** SEM-EDX experimental results on the surface of the Mg7Zn1Ag alloy following the determination of corrosion resistance by immersion tests in DMEM at 10 days, after the removal of corrosion products

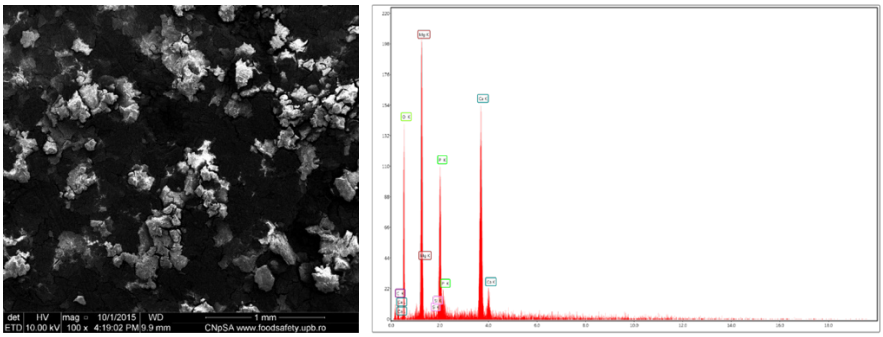

**Figure 6.28.** SEM-EDX experimental results on the surface of the Mg6Zn3Ag alloy following the determination of corrosion resistance by immersion tests in DMEM after 10 days, before the removal of corrosion products

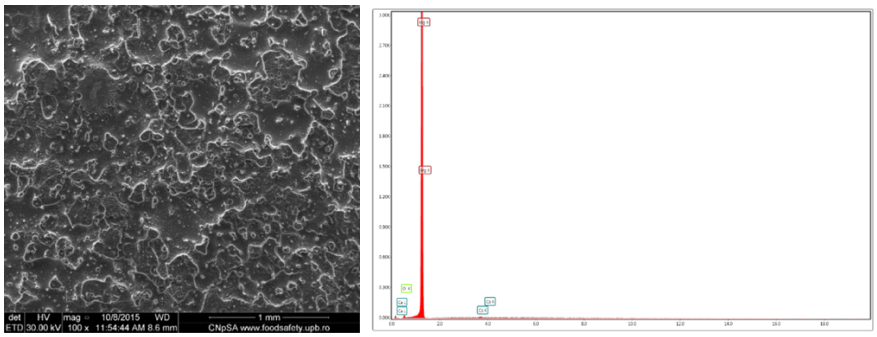

**Figure 6.29.** SEM-EDX experimental results on the surface of the Mg6Zn3Ag alloy following the determination of corrosion resistance by immersion tests in DMEM at 10 days, after the removal of corrosion products

Figures 6.30.-6.33 show the SEM images illustrating the surface of Mg7Zn1Ag and Mg6Zn3Ag samples covered with hydroxyapatite, after 10 days of immersion in SBF and DMEM media.

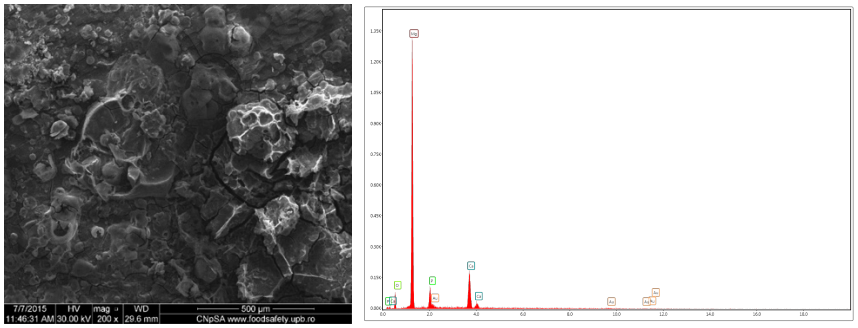

**Figure 6.30.** SEM-EDX experimental results on the surface of the coated Mg7Zn1Ag alloy (HA-Mg7Zn1Ag) following the determination of corrosion resistance by immersion tests in SBF after 10 days

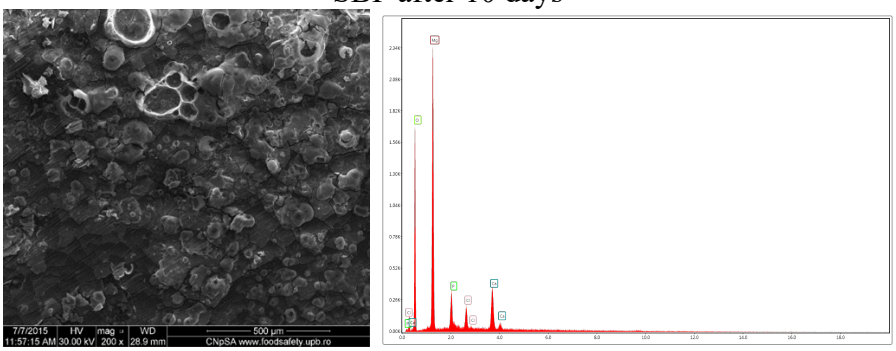

**Figure 6.31.** SEM-EDX experimental results on the surface of the coated Mg6Zn3Ag alloy (HA-Mg6Zn3Ag) following the determination of corrosion resistance by immersion tests in SBF after 10 days

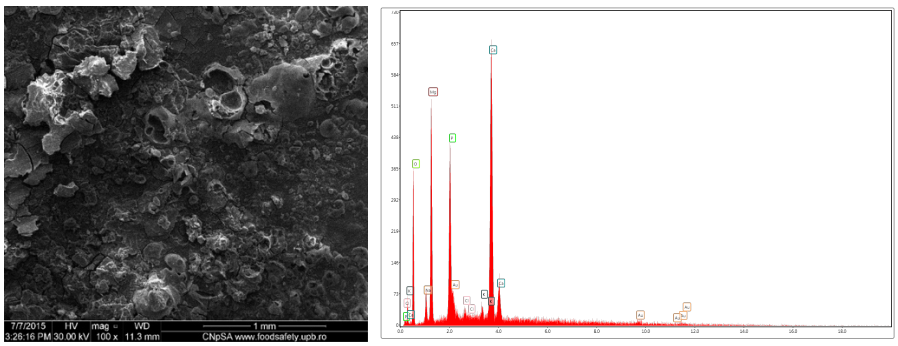

**Figure 6.32.** SEM-EDX experimental results on the surface of the coated Mg7Zn1Ag alloy (HA-Mg7Zn1Ag) following the determination of corrosion resistance by immersion tests in DMEM after 10 days

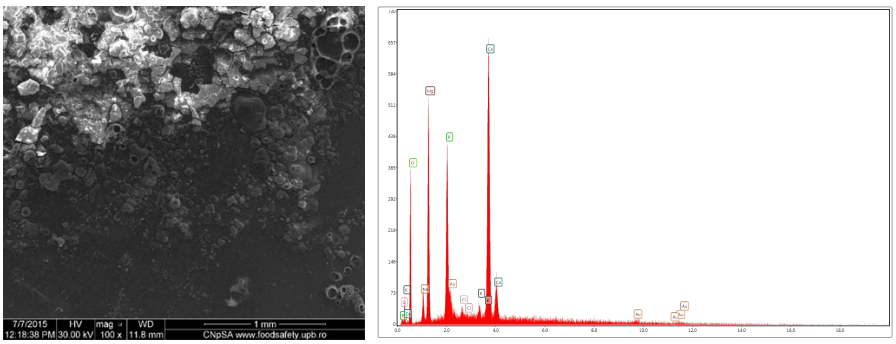

**Figure 6.33.** SEM-EDX experimental results on the surface of the coated Mg6Zn3Ag alloy (HA-Mg6Zn3Ag) following the determination of corrosion resistance by immersion tests in DMEM after 10 days

## 6.2. Determination of the biocompatibility of Mg-Zn-Ag alloys, before and after coating with hydroxyapatite

***Cell viability (MTT test)***

In the case of the extract made from Mg7Zn1Ag at the concentrations of 3.3% and 10%, no significant differences appeared compared to the control at 24 hours, but at 72 hours the cell viability decreases. The concentration of 30% induces a decrease in cell viability at 24 hours, but at 72 hours after incubation the cell viability increases, which indicates that during this interval the cells that survived in this environment were selected (Figure 6.34). The extracts of the Mg6Zn3Ag alloy did not produce significant changes in MSC viability at any of the time intervals tested, in this case viability being comparable to that of control cells.

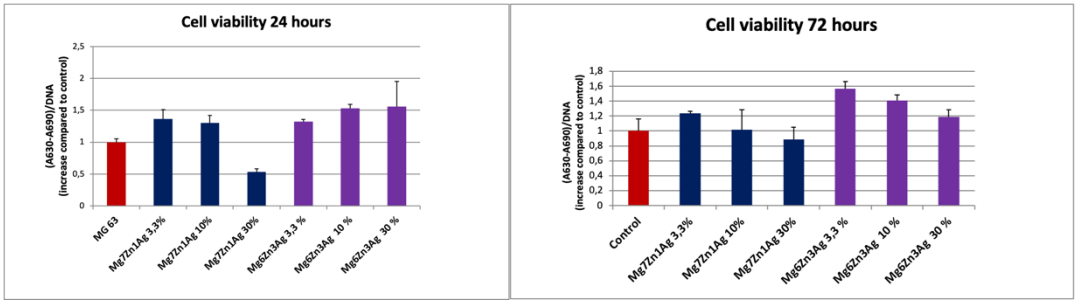


**Figure 6.34.** Viability of human mesenchymal stem cells recorded after their interaction with the extracts of the 2 alloys for 24 and 72 hours. The results were normalized by reference to the values recorded for the control, represented by MSCs not interacted with the alloy extracts.

***Cell proliferation (DNA dosage)***

At 24 hours after incubation, MSC proliferation was not influenced by the concentrations of the extracts used, and no significant decrease in proliferation was recorded compared to the control in any of the cases tested.

In the case of the Mg7Zn1Ag extract, concentrations of 3.3% and 10% do not change MSC proliferation, which is similar to that of the control, but the concentration of 30% induces a decrease in cell multiplication.

The cells incubated for 72 hours with the Mg6Zn3Ag extract, regardless of the concentration used, showed a low proliferation compared to the control cells (Figure 6.35).

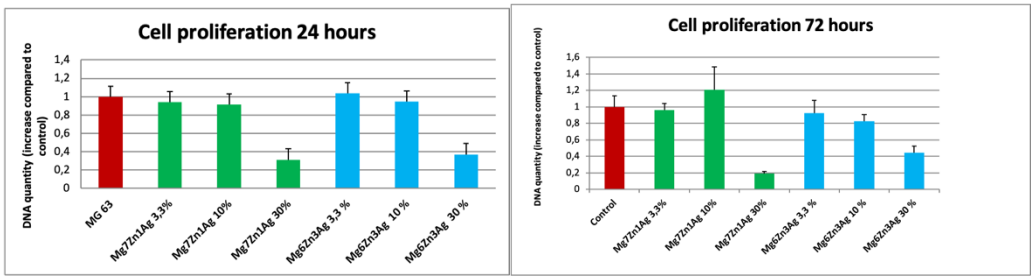


**Figure 6.35**. Proliferation of human mesenchymal stem cells recorded after their interaction with the extracts of the 2 alloys for 24 and 72 hours. The results were normalized by reference to the values recorded for the control, represented by MSCs not interacted with the alloy extracts.

***Determination of alkaline phosphatase activity***

Following this experiment, it was found that the alkaline phosphatase activity in MSCs cultured for 24 and 72 hours respectively in the extracts of Mg7Zn1Ag, Mg6Zn3Ag alloys was

comparable to that of the control cells. Only one exception was noted, that of the Mg7Zn1Ag extract which at the 30% concentration induced an increase in enzyme activity, the increase in activity being maintained even after 72 hours of incubation (Figure 6.36). At 72 hours in all other cases tested, an enzyme activity comparable to that at 24 hours was recorded, regardless of the concentration of extract used, this being also observed in the case of control cells.

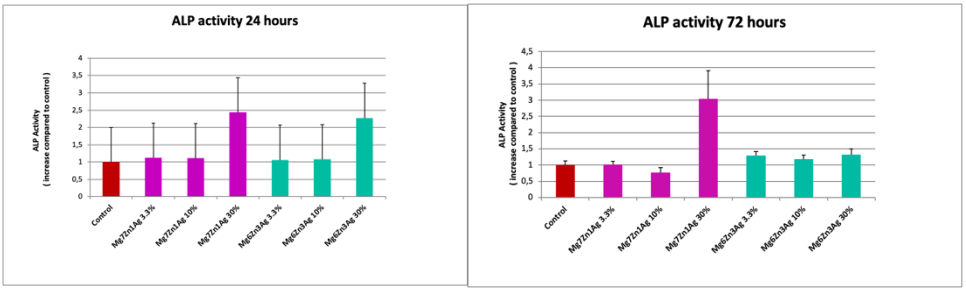


**Figure 6.36.** Alkaline phosphatase activity of MSCs recorded after their interaction with the extracts of the 2 alloys for 24 and 72 hours. The results were normalized by reference to the values recorded for the control, represented by MSCs not interacted with the alloy extracts.

***<u>Determination of the transcription level of the genes of interest by PCR (polymerization chain reaction)</u>***

*Modulation of osteoprotegerin gene expression*

As can be seen in Figure 6.37, gene expression for osteoprotegerin in MSCs cultured for 24 and 72 hours, respectively, in the extracts made from the 2 alloys (Mg7Zn1Ag, Mg6Zn3Ag) remained at a lower level compared to the control cells regardless of the concentrations of the extracts used.

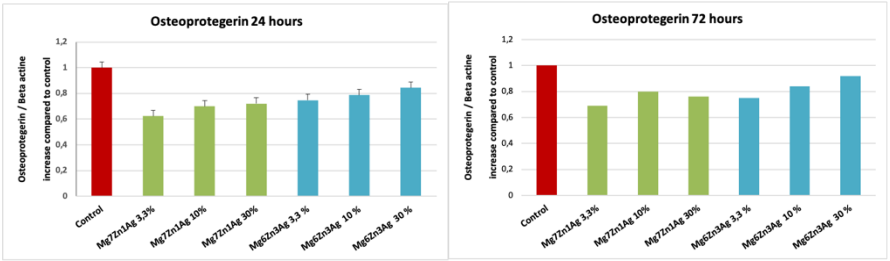


**Figure 6.37.** Transcription levels for the gene encoding osteoprotegerin, after 24 and 72 hours of MSC interaction with the extracts of the 2 alloys, respectively

*Modulation of type I collagen gene expression*

PCR experiments revealed that the expression of the type I collagen gene in MSCs incubated for 24/72 hours in the extracts of the 2 alloys remained at a low level compared to the control cells, the concentrations of the extracts not influencing in this case the collagen gene expression of type I (Figure 6.38).

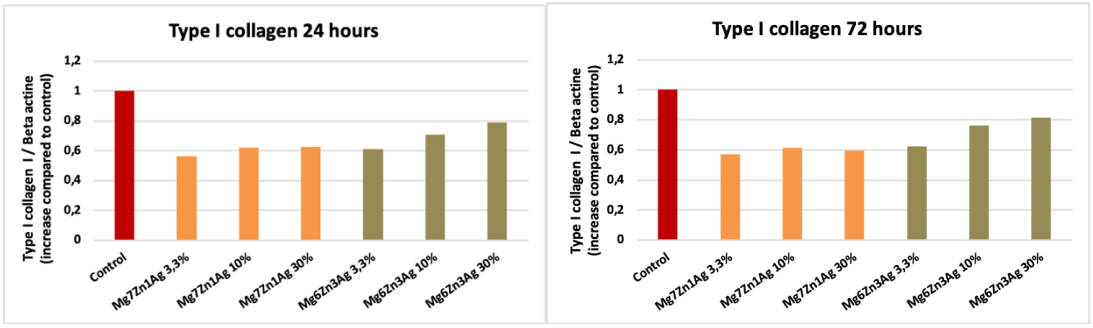


**Figure 6.38**. Transcript levels for the gene encoding type I collagen, after 24 and 72 hours of MSC interaction with the extracts of the 2 alloys, respectively

*Modulation of osteonectin gene expression*

As can be seen from Figures 6.39 and 6.40, gene expression for osteonectin and osteocalcin is lower compared to the control in MSCs incubated in the extracts of the 2 alloys. It can be seen that regardless of the concentrations of extracts used and the incubation time, the expression of these genes remained low, not being influenced by these two parameters.

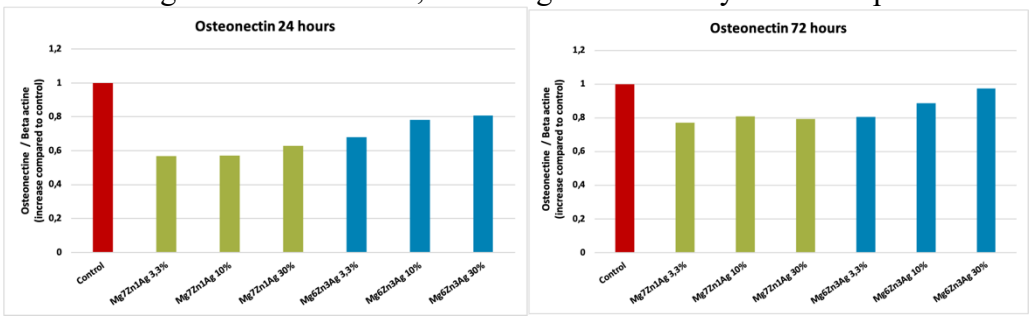


**Figure 6.39.** Transcript levels for the gene encoding osteonectin, after 24 and 72 hours of MSC interaction with extracts of the 2 alloys, respectively

*Modulation of osteocalcin gene expression*

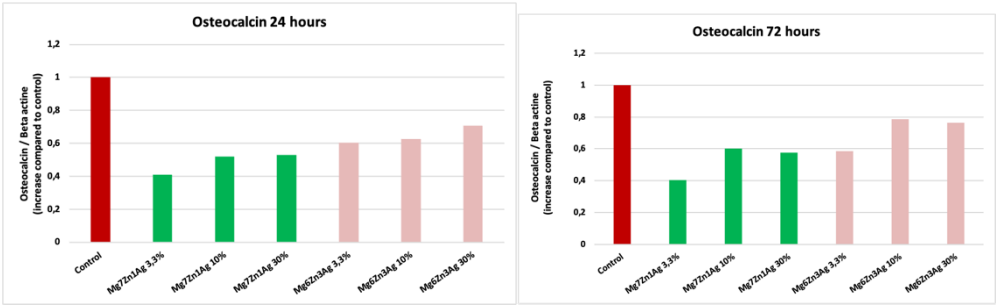


**Figure 6.40.** Transcript levels for the gene encoding osteocalcin, after 24 and 72 hours of MSC interaction with the extracts of the 2 alloys, respectively

Tests of cytotoxicity, proliferation, alkaline phosphatase activity, as well as gene expression for specific bone matrix constituents showed a good tolerance of osteoprogenitor cells to variable concentrations of degradation products of the studied alloys present in the eluate. Regarding the alkaline phosphatase activity, it was observed that it was increased in the case of MSC cells cultured for 24 and 72 hours respectively in the concentrated extract (30%) of the Mg7Zn1Ag alloy, although the proliferation of these cells was reduced compared to the control. Following these experiments, we can draw the following conclusion: the Mg6Zn3Ag

alloy extract induces the differentiation of MSCs towards osteoblasts and with the initiation of the differentiation process the proliferative capacity decreases.

***Determination of biocompatibility of hydroxyapatite coated Mg-Zn-Ag alloys. Cell viability (MTT assay)***

Considering the fact that the hydroxyapatite used to cover the experimental Mg-Zn-Ag alloys is biocompatible, and taking into account the complexity of the biocompatibility tests performed on the experimental Mg-Zn-Ag alloys, in the case of the experimental samples from Mg-Zn-Ag alloys coated with hydroxyapatite only an MTT assay was performed to assess cell viability.

The obtained experimental results are presented synthetically in figure 6.41.

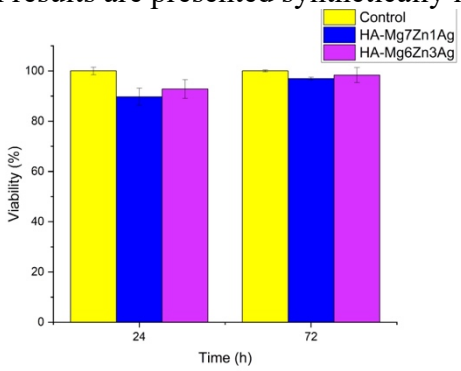


**Figure 6.41.** Viability of osteoblast cells after 1 and 3 days in extract collected after 24 hours from HA-Mg7Zn1Ag and HA-Mg-6Zn3Ag samples

According to the quantitative assessment of cytotoxicity, magnesium alloys from the Mg-Zn-Ag system covered with hydroxyapatite show viability values above 80%, which indicates their non-toxic character.

# CONCLUSIONS

## C1. General conclusions

Based on the theoretical studies and experimental research carried out in this doctoral thesis, the following general conclusions and assessments can be drawn:

- Magnesium alloys possess several advantages over the metallic materials used today in the execution of orthopaedic implants, such as stainless steels and titanium alloys, because they have mechanical properties similar to bone tissue, are biocompatible and are biodegradable. However, the rapid degradation of commercial magnesium alloys due to corrosion in the human environment limits clinical applications, as too high a degradation rate leads to premature deterioration of functionality in the human body.
- Research on biodegradable orthopaedic implants made of magnesium alloys is also stimulated by the existence of commercial biodegradable orthopaedic implants, namely the MAGNEZIX® bioresorbable compression screw (Syntellix AG, Hanover, Germany), made of Mg-Y-RE-Zr alloy, and the screw bioresorbable bone RESOMET/K-MET® (U&i Corporation, Seoul, Korea), made of Mg-Zn-Ca alloy. But at the same time, the development of new biodegradable implants that also have an antibacterial role is being pursued.

- The alloying elements influence both the chemical composition, in which case only the toxicological and systemic effect aspects on human cells are relevant, as well as the microstructure of magnesium alloys. If from a toxicological point of view, it is relatively simple to select a series of potential alloying elements, from the point of view of the effects of the addition of different alloying elements and their proportion on the structural characteristics it is much more complicated. If in the case of binary magnesium alloys the results of various research groups signal progress in the field, ternary magnesium-based alloy systems or complex ones with several alloying elements are still being evaluated.
- A major innovation in the field is the use of silver as an alloying element in the design of new magnesium alloys for biodegradable orthopaedic implants.
- The corrosion speed and also the degradation behaviour of magnesium-based alloys also depends on the surface properties. The influence of processing parameters and implant geometry on the functional properties and behaviour of orthopaedic implants during degradation are still being investigated.
- Biocompatibility and corrosion resistance must be considered as the first requirements for the development of new magnesium alloys for biodegradable orthopaedic implants, so that its degradation does not affect the biological functions of the body.
- As a result of the complex literature study carried out, the ternary alloys of the Mg-Zn-Ag system have a good potential to be used in the execution of biodegradable orthopaedic implants.
- It can be said that studies and research on hydroxyapatite coatings of biodegradable magnesium alloys, in order to reduce and control the rate of biodegradation, are a very current topic. The multitude of methods used to obtain hydroxyapatite coatings, as well as the fact that the phenomena taking place are not fully elucidated, support the fact that every contribution in this field will add to the development of this research .
- The properties of the hydroxyapatite layer deposited on biodegradable magnesium alloys and its adhesion to the substrate strongly depend on the selected deposition method and working conditions. The choice of a particular method depends on the functional requirements imposed on the layer, the maximum temperature that the substrate can withstand, the compatibility of the process with the processes applied to the substrate before and after deposition, and last but not least, the production costs, efficiency and large-scale manufacturing of the products.
- As a result of the complex literature study carried out, the use of the radiofrequency magnetron sputtering method for the deposition of hydroxyapatite layers on the surface of some biodegradable magnesium alloys appears to be an advantageous method in terms of deposition temperature, uniformity of the deposited layer and of the adhesion of the deposited layer to the substrate.

## C2. Original contributions

The carried-out research brought a series of novel contributions through the original results obtained and through their theoretical interpretation.

The original contributions will be presented in the following together with the most important results obtained.

1. As a result of the complex literature study carried out, design criteria for new magnesium alloys potentially usable as orthopaedic biomaterials have been established. Two new magnesium-based alloys from the Mg-Zn-Ag ternary system potentially usable as orthopaedic biomaterials (Mg7Zn1Ag and Mg6Zn3Ag, respectively) were obtained.
2. A complex characterization of the structure of the experimental alloys in the Mg-Zn-Ag system was carried out using modern methods and equipment, through optical microscopy,

scanning electron microscopy (SEM) coupled with EDS spectrometry and X-ray diffraction (XRD).

3. A surface modification of the experimental magnesium alloys Mg7Zn1Ag and Mg6Zn3Ag was designed and applied by depositing thin layers of hydroxyapatite using the magnetron sputtering method in the radio frequency regime, to improve the functional characteristics.
4. A complex characterization of the deposited hydroxyapatite layer was performed, both structurally and of the adhesion of the deposited layer and of the surface properties, using modern analysis methods: XRD, FTIR, SEM, EDS, AFM, profilometry, scratch-test, contact angle.
5. A complex test was performed to demonstrate the functional properties of the experimental materials: magnesium alloys from the Mg-Zn-Ag system (Mg7Zn1Ag and Mg6Zn3Ag), respectively magnesium alloys from the Mg-Zn-Ag system coated with hydroxyapatite by the spraying method magnetron in radio frequency regime (HA-Mg7Zn1Ag and HA-Mg6Zn3Ag).
6. Complex functional testing of both Mg-Zn-Ag magnesium alloys and hydroxyapatite-coated Mg-Zn-Ag magnesium alloys was performed by evaluating biodegradation and corrosion resistance by determining the amount of hydrogen released, by immersion tests and electrochemical tests, in two different test environments (SBF and Dulbecco).
7. The fact that the test environment decisively influences the results of corrosion resistance in the case of biodegradable Mg-Zn-Ag alloys has been highlighted. The performance of these tests in different environments (SBF and Dulbecco), as well as the use of scanning electron microscopy SEM coupled with EDS spectrometry as a method to qualitatively evaluate the effects of the test environment on the experimental samples, allowed important contributions to be made to strength evaluation studies to corrosion of biodegradable Mg-Zn-Ag magnesium alloys.
8. We can also say that the hydroxyapatite coating leads to the modification of the corrosion rate, regardless of the type of alloy in the Mg-Zn-Ag system.
9. Cytotoxicity tests were performed, which demonstrated that the experimental materials from the Mg-Zn-Ag magnesium alloy system are biocompatible and usable in the execution of temporary orthopedic implants for fracture fixation. Hydroxyapatite coating of these experimental alloys fully preserves and even improves the biocompatibility characteristics, according to *in vitro* tests performed on cell cultures. Obviously, for the full validation and further certification of these experimental alloys of the Mg-Zn-Ag system, it is necessary to carry out complete *in vivo* biocompatibility tests in animal models in the future.
10. The set of studies carried out allows us to conclude that the main objective of the doctoral thesis was fulfilled, i.e. the potential of some innovative magnesium alloys, from the Mg-Zn-Ag magnesium alloy system (Mg7Zn1Ag and Mg6Zn3Ag), was evaluated to be usable in the execution of osteosynthesis implants. It was also demonstrated the positive effect induced by the coating of these Mg-Zn-Ag magnesium alloys with hydroxyapatite, by the magnetron sputtering method in radio frequency mode at a deposition temperature of 300°C, on their biodegradation and biocompatibility characteristics.

## C3. Prospects for further development

This doctoral thesis has prospects for further development in several directions.

Thus, it is possible to expand studies on the antibacterial role of experimental magnesium alloys from the Mg-Zn-Ag system.

Further research can be developed on improving the functionalization methods of magnesium alloys, by adding specific proteins or growth factors, as well as embedding in the deposited layers some drugs.

Obviously, it is possible to extend research on *in vitro* and *in vivo* biocompatibility testing to specific animal models.

Also, the role played by the hydroxyapatite coating in terms of the evolution of the degraded surfaces in terms of the compounds that are formed on the surface can be evaluated more precisely in the case of animal model biocompatibility tests.

# VALUATION OF THE RESEARCH RESULTS

**Articles in ISI indexed and rated journals in the field of the PhD thesis**

**1. L. Dragomir (Nicolescu),** I. Antoniac, V. Manescu (Paltanea), A. Antoniac, M. Miculescu, O. Trante, A. Streza, C. M. Cotruț, D. A. Forna, *Microstructure and Corrosion Behaviour of Mg-Ca and Mg-Zn-Ag Alloys for Biodegradable Hard Tissue Implants*, Crystals **2023**, 13(8), 1213 (Q2, IF = 2,7).

**2. L. Dragomir (Nicolescu),** A. Antoniac, V. Manescu (Paltanea), A. Robu, M. Dinu, I.Pana, C.M.Cotruț, E. Kamel, I. Antoniac, J.V. Rau, A. Vladescu (Dragomir), *Preparation and characterization of hydroxyapatite coating by magnetron sputtering on Mg–Zn–Ag alloys for orthopaedic trauma implants*, Ceramics International, 49(16), 2023, 26274-26288 (Q1, IF = 5,2).

**Attendance at international conferences:**

**1. L. Nicolescu**, A. Antoniac, I. Antoniac- *Influence of testing environment on the degradation behaviour of magnesium alloys for orthopaedic implants* - eCM 2023, Bone and Fracture Repair, 10-12 iulie 2023, Davos Platz, Switzerland.

**2.** A. Robu, I. Antoniac, V. Mănescu (Păltânea), R. Bololoi, **L. Nicolescu** - *Mechanical properties and in vitro degradation on biodegradable Mg-Zn-Ca alloys* - BioReMed 2023, 19-21 iulie 2023, Sibiu, România.

**3. L. Dragomir**, A. Robu, A. Antoniac, I. Antoniac, A. Vladescu, H. Dura, N. Forna, M. B. Cristea and I. Carstoc, *Biodegradation Evaluation of some Magnesium-based Alloys type Mg-Zn-Zr-Ag before and after Synthetic Hydroxyapatite Coating using RF-Magnetron Sputtering,* International Conference on Innovative Research, ICIR EUROINVENT, 26-27 mai 2022, Iași, România.

4. Antoniac, I. Antoniac, F. Miculescu, A. Robu, V. Manescu (Paltanea), **L. Dragomir (Nicolescu)**, C. Cotrut – *Degradation of Fluoride Conversion Coatings on Mg-3Nd Magnesium Alloys in NaCl Solution* – 9th International Conference on Materials Science and Technologies – RoMat 2022, 24-25 noiembrie, București, România.

5. C. Nicolescu , O. Iorga, F. Alexe , T.-V. Tiganescu, C. Munteanu , S. Lupescu, B. Istrate , **L. Dragomir (Nicolescu),** I. Antoniac, *Characterization of Microstructure and Mechanical Behavior of Al2O3 Coatings Deposited by Atmospheric Plasma Spraying Technique on Hardox Steel* - ROMAT 2022, 24-25 noiembrie, București, România.

6. C. Tecu, **L. Dragomir**, M. Güven Gok, C. Milea, A. Antoniac, G. Göller, I. Antoniac - *Effect of sintering temperature on structure and properties of some new hydroxyapatite based composites for bone tissue engineering* - 10th International Conference on Materials Science and Engineering – BRAMAT 2017, Brașov, România.

**Articles in journals that are not in the field of the doctoral thesis**

**1.** K. Earar, R. Grigoroiu, M. M. Scutariu, E. Vasile, A. Antoniac, **L. Dragomir**, S. Gradinaru, *Effect of the Sandblasting Process on the Surface Properties of Dental Zirconia*, Revista de Chimie, 68(7), 2017.

**2.** R. Adam, H. Orban, **L. Dragomir**, C. Milea, I. Antoniac, A. Barbilian, *Investigation of Biodegradation Behavior of an Mg-1Ca Alloy during In Vivo Testin*g, KEM 752, 2017, p.87–92.

**3.** I. Antoniac, **L. Dragomir**, I. Csaki, I.M. Mates, D. Vranceanu, *Potential of the magnesium powder as filler for biomedical composites*, Biomater Tissue Technol, 2017, DOI: 10.15761/BTT.1000105.

**International Scientific Awards**

**Best Poster Award** - *Biodegradation Evaluation of some Magnesium-based Alloys type Mg-Zn-Zr-Ag before and after Synthetic Hydroxyapatite Coating using RF-Magnetron Sputtering,* International Conference on Innovative Research, ICIR EUROINVENT, IASI, May, 26-27, 2022

## SELECTIVE REFERENCES


1. Tsakiris, V.; Tardei, C.; Clicinschi, F.M. Biodegradable Mg Alloys for Orthopedic Implants – A Review. *J. Magnes. Alloys* **2021**, *9*, 1884–1905, doi:10.1016/j.jma.2021.06.024.
2. Xu, T.; Yang, Y.; Peng, X.; Song, J.; Pan, F. Overview of Advancement and Development Trend on Magnesium Alloy. J. Magnes. Alloys **2019**, 7, 536–544, doi:10.1016/j.jma.2019.08.001.
3. Antoniac, I.; Miculescu, M.; Mănescu (Păltânea), V.; Stere, A.; Quan, P.H.; Păltânea, G.; Robu, A.; Earar, K. Magnesium-Based Alloys Used in Orthopedic Surgery. Materials **2022**, 15, 1148, doi:10.3390/ma15031148.
4. Cheng, C.; Song, K.; Mi, X.; Wu, B.; Xiao, Z.; Xie, H.; Zhou, Y.; xiuhua, guo; Liu, H.; Chen, D.; et al. Microstructural Evolution and Properties of Cu–20 Wt% Ag Alloy Wire by Multi-Pass Continuous Drawing. *Nanotechnol. Rev.* **2020**, *9*, 1359–1367, doi:10.1515/ntrev-2020-0108.
5. Liu, C.; Ren, Z.; Xu, Y.; Pang, S.; Zhao, X.; Zhao, Y. Biodegradable Magnesium Alloys Developed as Bone Repair Materials: A Review. *Scanning* **2018**, *2018*, e9216314, doi:10.1155/2018/9216314.
6. Zhang, L.-N.; Hou, Z.-T.; Ye, X.; Xu, Z.-B.; Bai, X.-L.; Shang, P. The Effect of Selected Alloying Element Additions on Properties of Mg-Based Alloy as Bioimplants: A Literature Review. *Front. Mater. Sci.* **2013**, *7*, 227–236, doi:10.1007/s11706-013-0210-z.

7. Li, X.; Liu, X.; Wu, S.; Yeung, K.W.K.; Zheng, Y.; Chu, P.K. Design of Magnesium Alloys with Controllable Degradation for Biomedical Implants: From Bulk to Surface. *Acta Biomater.* **2016**, *45*, 2–30, doi:10.1016/j.actbio.2016.09.005.
8. Li, D.; Zhang, D.; Yuan, Q.; Liu, L.; Li, H.; Xiong, L.; Guo, X.; Yan, Y.; Yu, K.; Dai, Y.; et al. In Vitro and in Vivo Assessment of the Effect of Biodegradable Magnesium Alloys on Osteogenesis. *Acta Biomater.* **2022**, 141, 454–465, doi:10.1016/j.actbio.2021.12.032.
9. Zhang, B.; Hou, Y.; Wang, X.; Wang, Y.; Geng, L. Mechanical Properties, Degradation Performance and Cytotoxicity of Mg–Zn–Ca Biomedical Alloys with Different Compositions. *Mater. Sci. Eng. C* **2011**, 8, 1667–1673, doi:10.1016/j.msec.2011.07.015.
10. Bairagi, D.; Mandal, S. A Comprehensive Review on Biocompatible Mg-Based Alloys as Temporary Orthopaedic Implants: Current Status, Challenges, and Future Prospects. *J. Magnes. Alloys* **2022**, 10, 627–669, doi:10.1016/j.jma.2021.09.005.
11. Hassan, S.F.; Islam, M.T.; Saheb, N.; Baig, M.M.A. Magnesium for Implants: A Review on the Effect of Alloying Elements on Biocompatibility and Properties. *Materials* **2022**, *15*, 5669, doi:10.3390/ma15165669.
12. Liu, Y.; Lu, B.; Cai, Z. Recent Progress on Mg- and Zn-Based Alloys for Biodegradable Vascular Stent Applications. *J. Nanomater.* **2019**, *2019*, e1310792, doi:10.1155/2019/1310792.
13. Wang, L.; Lu, W.; Qin, J.; Zhang, F.; Zhang, D. Microstructure and Mechanical Properties of Cold-Rolled TiNbTaZr Biomedical β Titanium Alloy. *Mater. Sci. Eng. -Struct. Mater. Prop. Microstruct. Process. - MATER SCI ENG -STRUCT MATER* **2008**, *490*, 421–426, doi:10.1016/j.msea.2008.03.003.
14. Kumar, R.; Katyal, P. Effects of Alloying Elements on Performance of Biodegradable Magnesium Alloy. *Mater. Today Proc.* **2021**, *56*, doi:10.1016/j.matpr.2021.08.233.
15. Mohammadi-Zerankeshi, M.; Alizadeh, R.; Labbaf, S. Improving Mechanical, Degradation and Biological Behavior of Biodegradable Mg–2Ag Alloy: Effects of Y Addition and Heat Treatment. *J. Mater. Res. Technol.* **2023**, *22*, 1677–1694, doi:10.1016/j.jmrt.2022.12.026.
16. Wang, Z.; Zeng, J.; Tan, G.; Liao, J.; Zhou, L.; Chen, J.; Yu, P.; Wang, Q.; Ning, C. Incorporating Catechol into Electroactive Polypyrrole Nanowires on Titanium to Promote Hydroxyapatite Formation. *Bioact. Mater.* **2018**, *3*, 74–79, doi:10.1016/j.bioactmat.2017.05.006.
17. Cao, L.; Ullah, I.; Li, N.; Niu, S.; Sun, R.; Xia, D.; Yang, R.; Zhang, X. Plasma Spray of Biofunctional (Mg, Sr)-Substituted Hydroxyapatite Coatings for Titanium Alloy Implants. *J. Mater. Sci. Technol.* **2019**, *35*, 719–726, doi:10.1016/j.jmst.2018.10.020.
18. Shikha, D.; Shahid, Md.; Sinha, S.K. Improvement in Adhesion of HAP Deposited on Alumina after Ar+ Ions Implantation and Its Physiochemical Properties. *Surf. Interfaces* **2020**, *19*, 100485, doi:10.1016/j.surfin.2020.100485.
19. Lenis, J.A.; Rico, P.; Ribelles, J.L.G.; Pacha-Olivenza, M.A.; González-Martín, M.L.; Bolívar, F.J. Structure, Morphology, Adhesion and in Vitro Biological Evaluation of Antibacterial Multi-Layer HA-Ag/SiO2/TiN/Ti Coatings Obtained by RF Magnetron Sputtering for Biomedical Applications. *Mater. Sci. Eng. C* **2020**, *116*, 111268, doi:10.1016/j.msec.2020.111268.
20. Ahmadi, R.; Afshar, A. In Vitro Study: Bond Strength, Electrochemical and Biocompatibility Evaluations of TiO2/Al2O3 Reinforced Hydroxyapatite Sol–Gel Coatings on 316L SS. *Surf. Coat. Technol.* **2021**, *405*, 126594, doi:10.1016/j.surfcoat.2020.126594.

21. Ling, L.; Cai, S.; Li, Q.; Sun, J.; Bao, X.; Xu, G. Recent Advances in Hydrothermal Modification of Calcium Phosphorus Coating on Magnesium Alloy. *J. Magnes. Alloys* **2022**, *10*, 62–80, doi:10.1016/j.jma.2021.05.014.
22. Lorenz, C.; Brunner, J.G.; Kollmannsberger, P.; Jaafar, L.; Fabry, B.; Virtanen, S. Effect of Surface Pre-Treatments on Biocompatibility of Magnesium. *Acta Biomater.* **2009**, *5*, 2783–2789, doi:10.1016/j.actbio.2009.04.018.
23. Antoniac, I.; Miculescu, F.; Cotrut, C.; Ficai, A.; Rau, J.V.; Grosu, E.; Antoniac, A.; Tecu, C.; Cristescu, I. Controlling the Degradation Rate of Biodegradable Mg–Zn-Mn Alloys for Orthopedic Applications by Electrophoretic Deposition of Hydroxyapatite Coating. *Materials* **2020**, *13*, 263, doi:10.3390/ma13020263.
24. Parau, A.C.; Dinu, M.; Cotrut, C.M.; Pana, I.; Vranceanu, D.M.; Constantin, L.R.; Serratore, G.; Marinescu, I.M.; Vitelaru, C.; Ambrogio, G.; et al. Effect of Deposition Temperature on the Structure, Mechanical, Electrochemical Evaluation, Degradation Rate and Peptides Adhesion of Mg and Si-Doped Hydroxyapatite Deposited on AZ31B Alloy. *Coatings* **2023**, *13*, 591, doi:10.3390/coatings13030591.
25. Quan, P.H.; Antoniac, I.; Miculescu, F.; Antoniac, A.; (Păltânea), V.M.; Robu, A.; Bița, A.-I.; Miculescu, M.; Saceleanu, A.; Bodog, A.D.; et al. Fluoride Treatment and In Vitro Corrosion Behavior of Mg-Nd-Y-Zn-Zr Alloys Type. *Materials* **2022**, *15*, 566, doi:10.3390/ma15020566.